3. CRATER MATERIALS

FIGURE 3.1 (OVERLEAF).—Craters on farside area centered at 20° S., 162° E., in Keeler-Heaviside basin (massifs of ring constitute horizon). Large complex crater in center is Keeler (169 km); smaller fresh crater on east (left) wall of Keeler is Planté (38 km); degraded crater in lower left is Stratton (71 km). Small simple craters include overlapping, aligned secondary craters between Keeler and Stratton, superposed on other materials. Compare figure 1.4. Apollo 12 frame H–4961.

3. CRATER MATERIALS

CONTENTS

INTRODUCTION

Stratigraphers have understandably devoted much attention to the deposits of craters, the most conspicuous lunar landforms (fig. 3.1). Much of the upper lunar crust consists of interfingering beds of crater material. Crater deposits provide more stratigraphic datum horizons for reconstructing lunar geologic history than do any other lunar materials, and large fresh craters can be relatively dated over extensive areas. Interpretations of basins and terra samples of basin deposits depend on knowledge of their smaller relatives, craters. The importance of craters and their deposits requires a detailed description here of their appearance and formative processes.

To some extent, crater materials can be mapped and relatively dated without knowledge of their origin. They obey the same basic laws of sedimentation as does terrestrial sediment, despite their radiation from randomly distributed point sources of energy (Mutch, 1970, p. 164). However, interpretation of the terrane beyond the obvious influence of a crater depends largely on knowledge of the crater's origin. On the Moon, the effects of an impact crater extend much farther than those of an endogenic crater of the same size. Craters lacking morphologies diagnostic of origin and age, therefore, have a different stratigraphic significance if they are degraded impact craters rather than separate genetic types. Thus, the question of crater origin occupies much of the next section.

Because impact is now known to be the main crater-generating process on the Moon, the rest of this chapter and this volume stresses impact craters. The section below entitled "Cratering Mechanics" discusses in detail how the distribution and interrelations of crater-material facies arose. The brecciated and melted products of impact are then described in general terms in preparation for later descriptions of the impact-generated geologic units that have been sampled. Finally, I summarize the origins of crater-material units as mapped geologically.

GENERAL FEATURES

Typical morphology

Individual primary-impact craters resemble one another more than they differ. Borrowing a term from stellar astronomy, Wilhelms and McCauley (1971) called the series of morphologically related craters the *main sequence*. The rims of these craters are nearly circular. Their floors lie below the level of the adjacent terrain. Their inner walls slope steeply, and the flank outside the raised rim crest slopes more gently. Systematic outward gradations of morphology reflect the effects of ejection and deposition of a three-dimensional, laterally continuous unit of inner-rim material and gradational outer deposits of secondary craters. Main-sequence craters are randomly scattered over a given terrain in numbers inversely proportional to crater diameter.

In general, lunar craters increase in morphologic complexity with increasing size (figs. 3.1, 3.2). The size-morphology series is not entirely gradational but undergoes a fairly abrupt discontinuity at crater diameters of about 16 to 21 km (fig. 3.3; Pike, 1974, 1980a, b, c). Smaller fresh craters have simple, smooth interior profiles, smooth and highly circular rim crests, and depth/diameter (*d/D*) ratios of about 1/5 (table 3.1). Their floors are commonly flat or gently sloping and are evidently composed of rubbly or fine debris accumulated from the walls (fig. 3.2*B*). Many ejecta blankets of the younger craters of this relatively simple type display radial textures; some have subconcentric dunelike forms (fig. 3.2*A*).

Larger craters are more complex (figs. 3.2*C–E*, 3.4). In unmodified form, they have one or more of the following interior features: (1) a broad floor that is generally level but is interrupted by various hills and mounds; (2) a centrally disposed hill, peak, or peak complex; (3) single or multiple blocks or slices of material slumped from the walls; (4) continuous terraces on the wall that represent

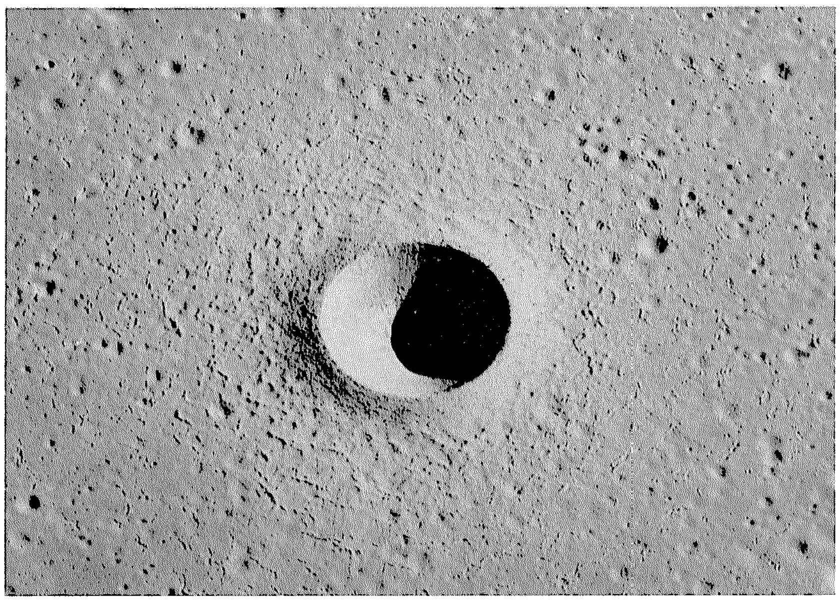

A

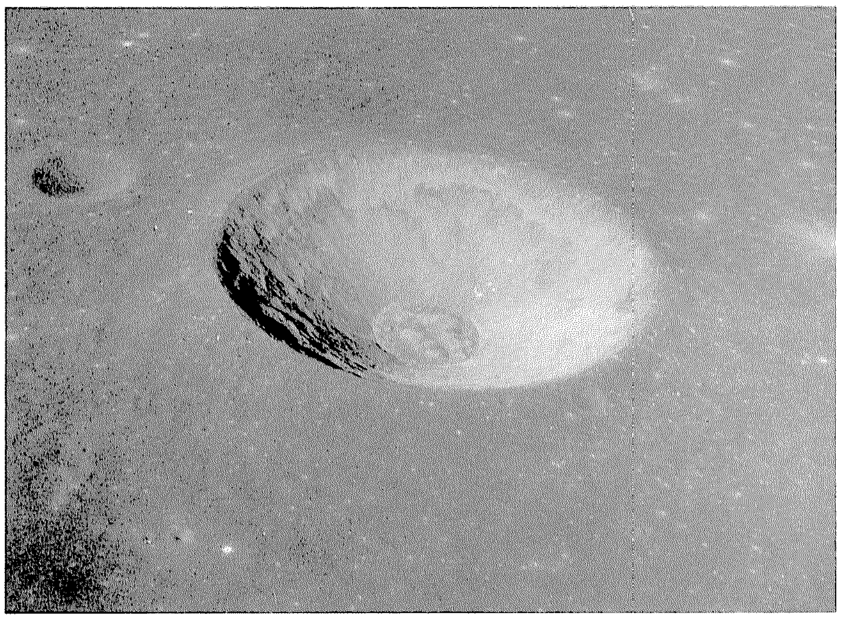

B

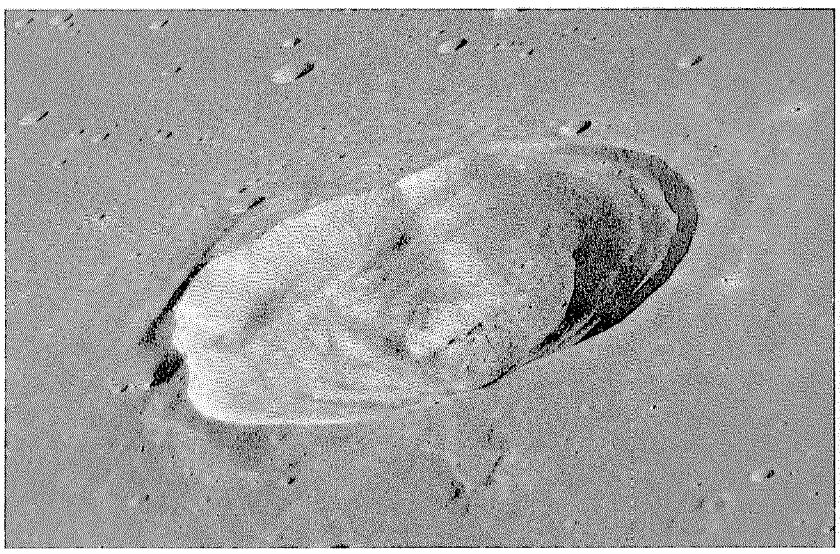

C

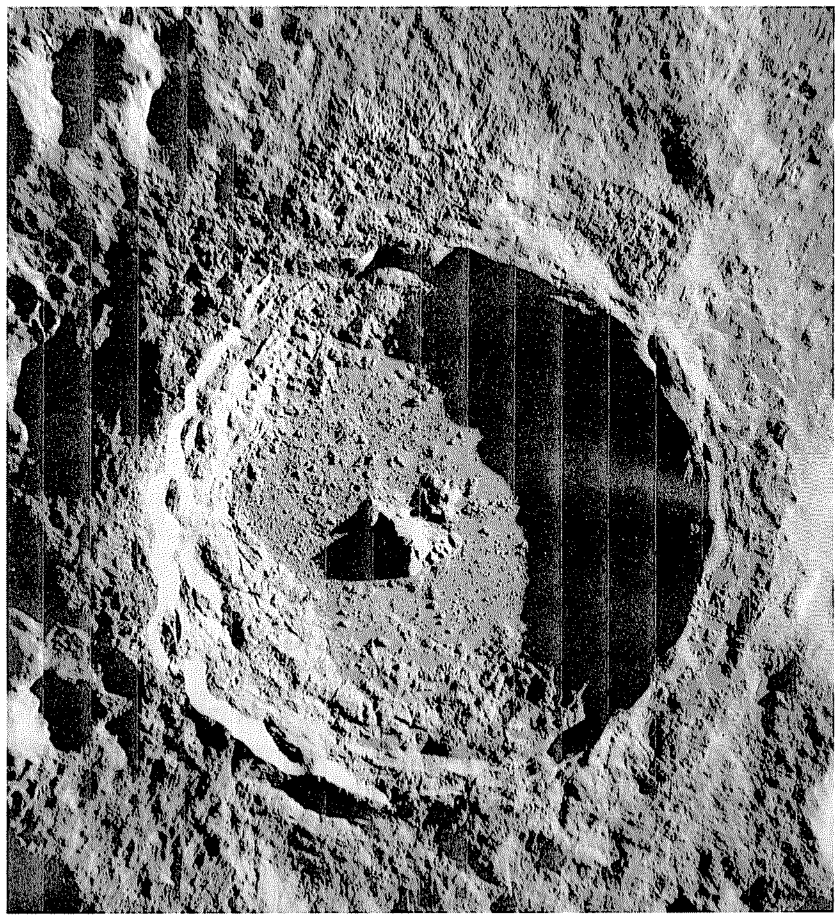

D

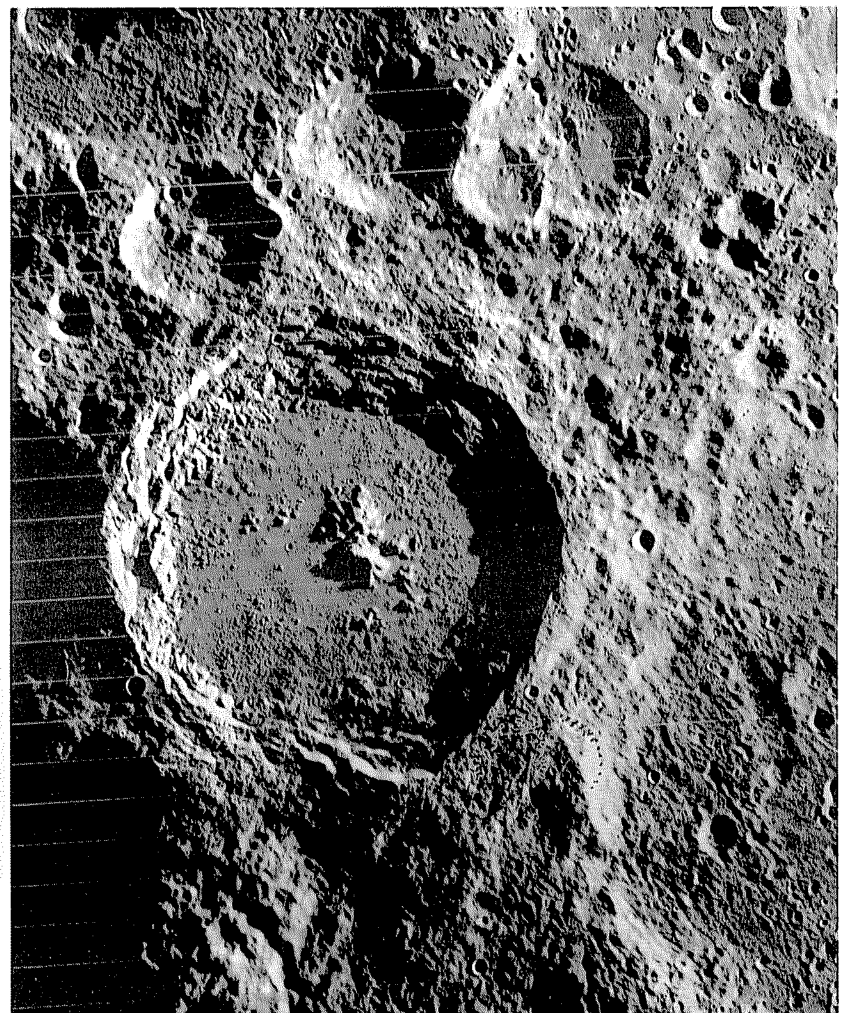

E

FIGURE 3.2.—Simple and complex lunar impact craters.

A. Linné (2.5 km, 28° N., 12° E.). Interior profile is smooth except for minor rubble; ejecta is subconcentric and dunelike. Apollo 15 frame P–9353.

B. Taruntius H (8.5 km, 0.5° N., 50° E.). Profile is smooth except for level floor, composed of rubble from walls; rim appears smooth, though not favorably illuminated in this photograph. Apollo 10 frame H–4253.

C. Arago (26 km, 6° N. 21° E.). Large wall terraces, evidently formed by slumping; peak and wall merge. Apollo 10 frame H–4630.

D. Tycho (85 km, 43° S., 11° W.). Characterized by very crisp, fresh-appearing topography much more complex than that of Arago. Floor mounds are fissured. Pools of impact melt are superposed on terraces and rim flank; radial flow texture of interior and exterior melt is also visible. Concentric inner-rim texture grades to radial outer texture. Orbiter 5 frame M–125.

E. Hausen (167 km, 66° S., 88° W.). Floor is broader relative to diameter than in Tycho; peak is relatively smaller, though large absolutely. Possible ringlike pattern of smaller peaks is visible. Terraces and hummocky wall masses are conspicuous. Secondary craters and herringbone pattern are conspicuous north and southeast of crater. Orbiter 4 frame H–193.

TABLE 3.1.—*General crater-identification criteria*

[Contributions from Richard J. Pike]

Property	Primary impact	Secondary impact	Endogenic
Size	Any	Mostly <30 km in diameter; proportional to size of source	Mostly <<20 km in diameter.
Slope of size-frequency curve (cumulative)	-1.9 for postmare craters <2 km in diameter	-3.6 to -4.0	About -2 (Greeley and Gault, 1979).
Circularity[1]	Circular, <15-20 km in diameter; crenate, >20 km in diameter ($0.70 \leq C \leq 0.95$; median, 0.82).	Varies ($0.35 \leq C \leq 0.75$; median, 0.54)	Varies ($0.35 \leq C \leq 0.85$; median, 0.55).
Depth	Much deeper than surrounding terrain where unmodified	Shallow except far from source	Varies; floor commonly near level of surrounding terrain.
Interior profile	Simple, 16-21 km in diameter; complex, >16-21 km in diameter.	Featureless except where filled	Varies.
Rim-flank profile	Rugged near crest, then concave to 2 radii	Inconspicuous except in large craters	Varies; mostly smooth and low.
Rim-flank texture	Concentric, hummocky near crest; radial to about 1 radius.	V-shaped or linear intercrater ridges	Inconspicuous.
Ejecta distribution	Mostly symmetrical (but see fig. 3.11A)	Directed away from source	Widespread.
Mutual relations	Interference features (fig. 3.14A) or "pushthrough" (fig. 3.25) rare.	Interference features common; downrange overlap common (fig. 3.4F).	Varies.
Spatial distribution	Random on a geologic unit except for rare pairs or triplets (fig. 3.14).	Concentrated about source in clusters, chains, or loops; commonly radial to basins; on bright rays when young.	Amid dark material, on domes, or aligned on rilles.

[1]Circularity (C) is defined as the ratio of the area of the inscribed circle to that of the circumscribed circle (fitted to planimetric outline of rim crest).

wholesale circumferential failure of the rim, as opposed to the blocks or slumps or to the minor debris wasting seen in simple craters; and (5) a *d/D* ratio that varies with diameter, from about 1/5 for small complex craters to about 1/40 for the largest (fig. 3.3; Pike, 1980c). Their rims are scalloped or irregular, though still more or less radially symmetrical; some of the scallops are the source areas of the wall blocks or terraces (fig. 3.2*C*).

Exterior features are also better developed in large than in small craters. Rim topography adjacent to the crest and out to about half a crater radius is elevated, rugged, and commonly concentrically structured (figs. 3.2*D*, *E*). Ejecta is lower and more radially structured beyond this rugged collar. Between one and two radii from the crest, the radial pattern passes into a zone dominated by negative landforms, the secondary craters. Whereas the interior features of small and large craters differ in origin, the exterior features of all craters are similar in origin. Following Dence (1964, 1965), *simple* and *complex* are used here as technical terms for the two size-related morphologic classes.

Secondary-impact craters

Secondary-impact craters differ in most respects from their parents (table 3.1). Sizes are controlled not by the nearly unrestricted masses and kinetic energies of cosmic fragments but by the size of the primary crater and the 2.4-km/s lunar escape velocity, above which the ejected fragments would leave the Moon. Because of the lower impact velocities, rim-crest circularity is less commonly developed than in hypervelocity primaries (fig. 3.4). However, circular secondaries do form at large distances from their sources (fig. 3.5) and are difficult to distinguish from primaries if not clustered. Because the ejecta projectiles that form secondaries are larger relative to crater size than the hypervelocity cosmic projectiles, irregularities in projectile shape are more manifest in secondaries than in primaries. In addition, unbonded debris may create secondary craters (Schultz and Mendenhall, 1979). Most interior profiles of secondaries are as smooth

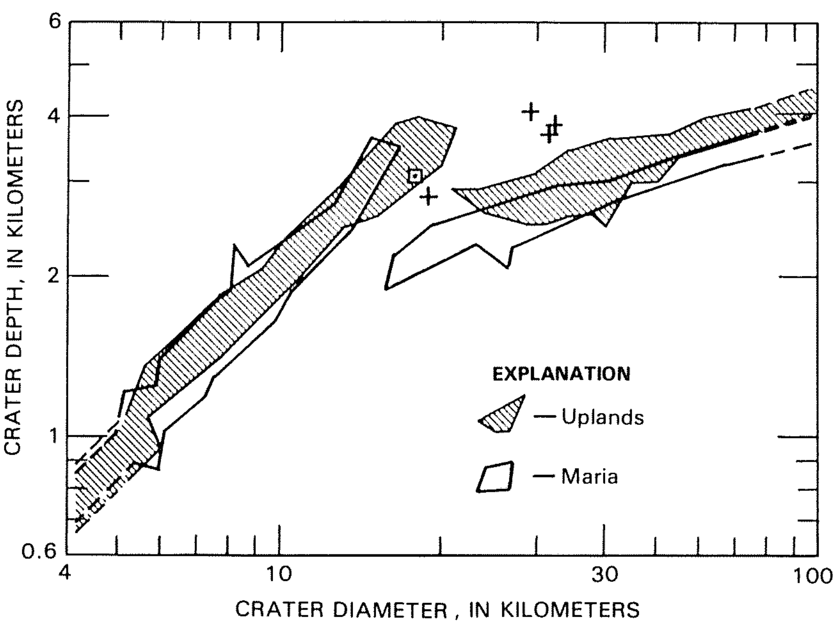

FIGURE 3.3.—Depth-diameter (*d/D*) ratios of simple craters (steep slopes, left) and complex craters (shallow slopes, right), including 136 craters on lunar terrae (uplands) and 203 craters on lunar maria; craters 4.2 to 95 km in diameter are plotted. Simple-to-complex transition occurs at about 21-km diameter in terrae and at 16-km diameter in maria. Complex craters show greater differences in *d/D* ratio in the two substrates than do simple craters. Square and crosses denote craters with transitional morphologies. From Pike (1980a, fig. 9).

as or smoother than those of small primaries, but shallower (Pike and Wilhelms, 1978). Ejected blocks are uncommon, and the exterior textures of individual secondaries are also smoother than those of primaries. Ejecta of grouped secondaries, however, may be texturally complex (figs. 3.4*C*–*F*, 3.6).

Spatial grouping is the main difference from primaries and is the main diagnostic characteristic of secondary-impact craters. Whereas primaries are randomly grouped, secondaries are highly concentrated. Secondaries generally occur in linear or curving chains or in patches and clusters. Only a few of the farflung projectiles may separate enough to form seemingly randomly scattered secondaries.

Secondaries may have revealed more about the cratering process than have the primary craters. Early investigators equipped with good photographs or observing the Moon visually with telescopes were impressed by the myriad small craters that are satellitic to large craters of the Copernicus type (fig. 3.4). What remains the most convincing set of arguments for the impact origin of both the satellitic and the primary craters was assembled at the beginning of the space age by Shoemaker (1962b). On the basis of an excellent telescopic photograph (fig. 3.4*A*), he mapped the satellitic craters of Copernicus (fig. 3.4*B*) and successfully accounted for their pattern by cratering and ballistic theory. He showed that the chains, loops, and clusters were probably excavated by secondary impacts of ejecta derived from certain structures in the bedrock struck by the Copernicus primary impact. His analysis was supported afterward by field study of ray loops formed from an identifiable bed in the target rock of one of the fresh Henbury meteorite craters in Australia (Milton and Michel, 1965), by laboratory experiments (Gault and others, 1968b), and by examination of high-velocity to hypervelocity missile-impact craters in natural materials (Moore, 1971, 1976).

Although primary impact of an object from space followed by secondary impact of the resulting ejecta was shown to be consistent with the lunar and terrestrial patterns of satellitic craters, other mechanisms continued to be invoked. An explosive origin by the sudden release of accumulated volcanic gases could theoretically explain the patterns except for the enormous energy required, estimated for Copernicus by Shoemaker (1962b, p. 333) at 7.5×10^{21} J. Such energies could not accumulate in a planetary crust because the weak rocks could not contain them without premature release (Taylor, 1982, p. 63). Endogenic mechanisms fail abjectly to explain the ray pattern of Tycho, part of which extends to the limbs of the Moon (fig. 3.6) and thus would require enormous internal energies or global-scale fault or fissure systems centered about a point. One advocate of such structural systems (Alter, 1963) realized that an impact must have formed Tycho but postulated that the secondaries formed endogenically along impact-opened cracks, because the rays are not exactly radial.

This offcenter relation of the rays was among the first arguments for internal origin to be finally refuted by Lunar Orbiter photography in 1967. Shoemaker (1962b, 1964; Shoemaker and Hackman, 1962, p. 290), Baldwin (1963, p. 355), the "endogenist" Firsoff (1961), and the impact-plus-endogeny proponent Alter (1963) had all noted that the nonradial rays consist of elements which are individually radial to the primary crater and which commonly originate at secondary craters (fig. 3.4*A*). Orbiter photographs show that the ray elements coincide with ridged ejecta of the secondary craters that was cast away from the primary crater; the secondary-crater ejecta has a herringbone or bird's-foot pattern (figs. 3.4*C*–*F*, 3.6). Septa divide many crater pairs, as they do several of the Henbury craters (Milton and Michel, 1965; Milton, 1968b). In a major advance, the ridges, herringbone pattern, septa, and even domelike features were closely

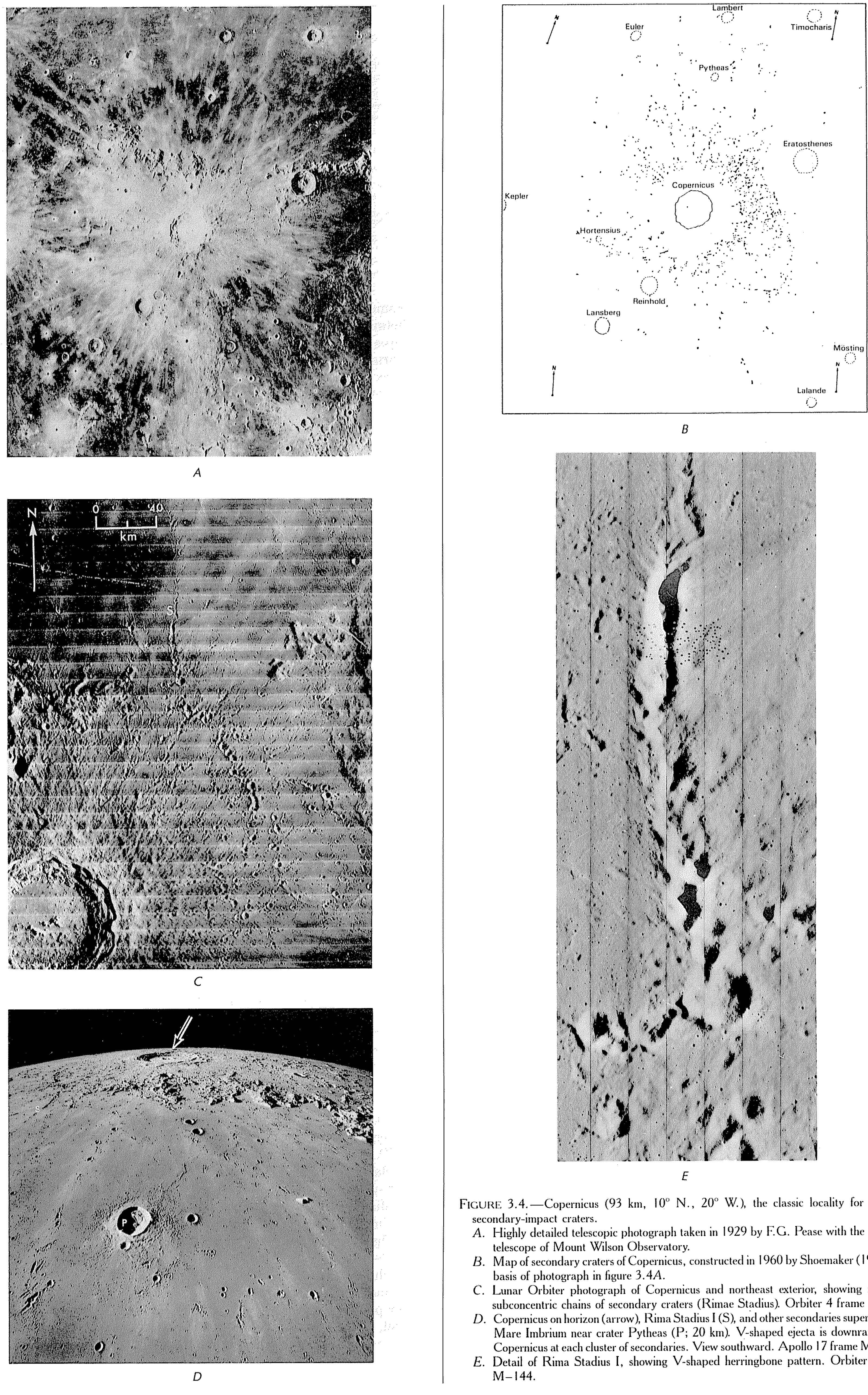

FIGURE 3.4.—Copernicus (93 km, 10° N., 20° W.), the classic locality for study of secondary-impact craters.

A. Highly detailed telescopic photograph taken in 1929 by F.G. Pease with the 100-inch telescope of Mount Wilson Observatory.

B. Map of secondary craters of Copernicus, constructed in 1960 by Shoemaker (1962b) on basis of photograph in figure 3.4*A*.

C. Lunar Orbiter photograph of Copernicus and northeast exterior, showing rays and subconcentric chains of secondary craters (Rimae Stadius). Orbiter 4 frame H–121.

D. Copernicus on horizon (arrow), Rima Stadius I (S), and other secondaries superposed on Mare Imbrium near crater Pytheas (P; 20 km). V-shaped ejecta is downrange from Copernicus at each cluster of secondaries. View southward. Apollo 17 frame M–2444.

E. Detail of Rima Stadius I, showing V-shaped herringbone pattern. Orbiter 5 frame M–144.

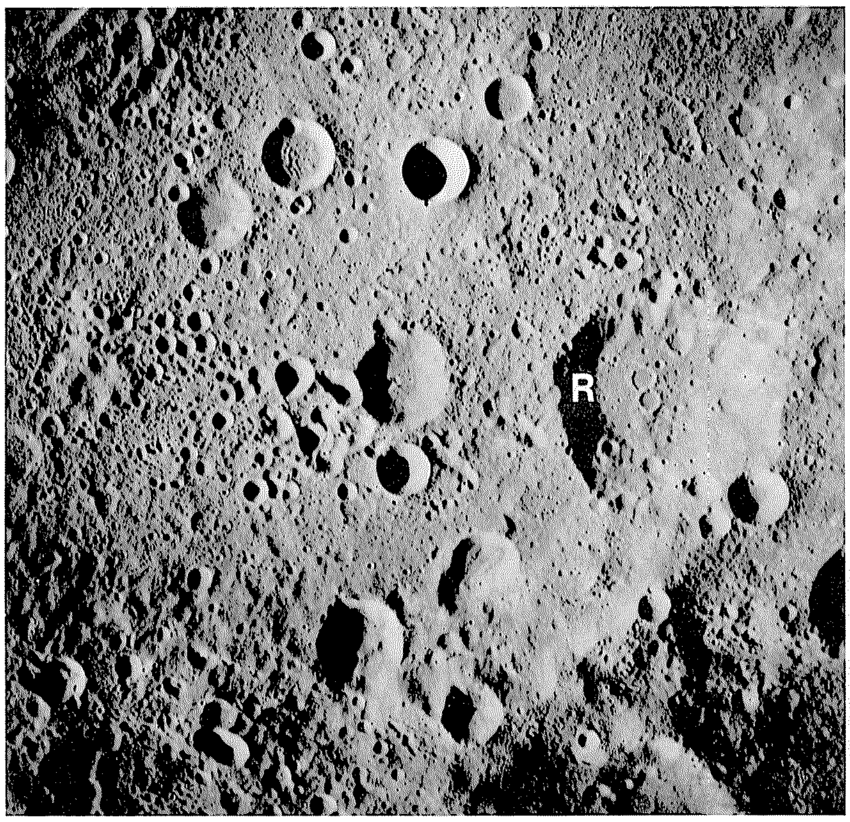

imitated in laboratory experiments (fig. 3.7) by Oberbeck and Morrison (1973a, b, 1974). The intersection angles of the lunar V-shaped ridges were fully modeled by various spacings and timings of nearly simultaneous artificial impacts that caused cones of crater ejecta to interact complexly upon collision. Ironically, some of the grossly off-center satellitic chains that have the classic herringbone pattern modeled by Oberbeck and Morrison are the Stadius chains east of Copernicus (figs. 3.4*C–E*), which were interpreted by some of the most astute proponents of lunar impact before the Orbiter photography as volcanic (Shoemaker, 1962b, p. 302; Shoemaker and Hackman, 1962, p. 298; Baldwin, 1963, p. 378; Schmitt and others, 1967).

FIGURE 3.5.—Group of small circular craters (left center) in crater Gagarin (272 km, 20° S., 149° E.; compare fig. 1.4) are secondary to a distant crater. Largest crater superposed on Gagarin rim is Raspletin (R; 49 km), presumably a primary. Apollo 15 frame M–293.

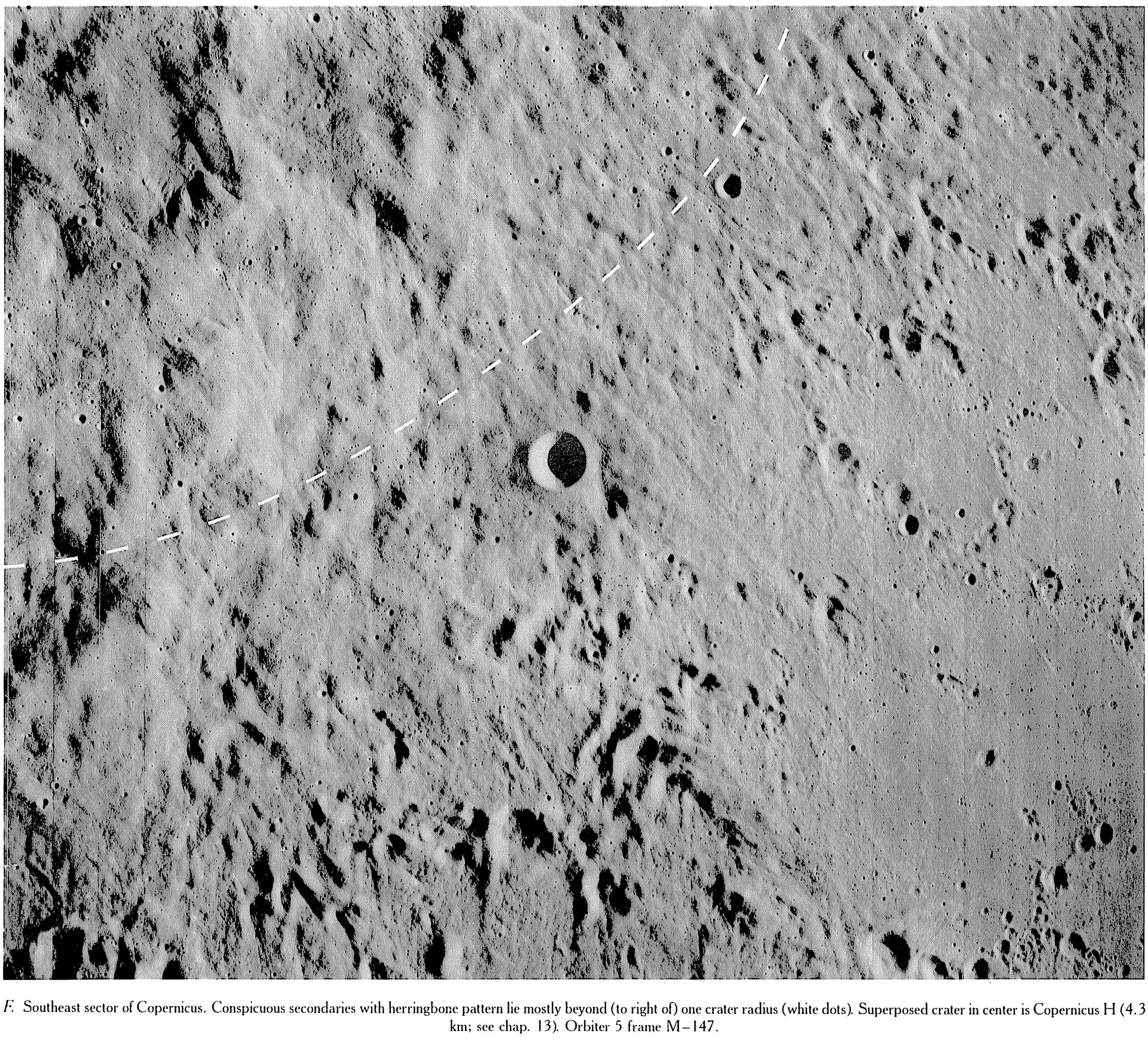

F. Southeast sector of Copernicus. Conspicuous secondaries with herringbone pattern lie mostly beyond (to right of) one crater radius (white dots). Superposed crater in center is Copernicus H (4.3 km; see chap. 13). Orbiter 5 frame M–147.

Only the most obdurate endogenists (Green, 1971; McCall, 1980) could still believe in the volcanic origin of such craters as Copernicus and Tycho or their satellitic craters after 1967. Secondary-impact origin was also readily extrapolated to larger-scale associations, for example, the 180-km-diameter primary crater Petavius and its retinue of small craters (Hodges, 1973b). For larger craters, volcanic and tectonic interpretations continued to appear for several years. A secondary-impact origin was recognized for many, but not all, satellitic craters (max 10 km diam) of the 260-km-diameter Iridum crater (fig. 3.8; Ulrich, 1969; Scott and Eggleton, 1973). The satellitic craters of the Orientale basin (fig. 3.9) were recognized as secondary-impact craters by some geologists (Offield, 1971; Wilhelms and McCauley, 1971) but were interpreted endogenically by others well into the period of Apollo exploration (for example, Karlstrom, 1974). Internal origins were widely favored for seemingly noncompound craters larger than 5 km in diameter whose rims have such irregularities as straight segments or reentrants (fig. 3.10*C*; Wilhelms and McCauley, 1971).

Several systematic relations support the secondary-impact origin for all these satellitic craters, of all sizes. The size ratios and spatial relations of secondaries to primaries remain much the same around primaries ranging in diameter from 1 km (Oberbeck and others, 1974) to more than 1,000 km (ringed basins; Wilhelms, 1976; Wilhelms and others, 1978). The ratios of the largest satellitic-crater diameters to the primary-crater diameter decrease relatively little, from about 0.05 for 100-km-diameter primaries (Shoemaker, 1965, p. 121), through 0.04 for the Iridum crater (Scott and Eggleton, 1973), to about 0.02 for large basins (Wilhelms and others, 1978). Size-frequency distributions of satellitic craters also are remarkably similar over a wide size range; cumulative plots of craters satellitic to nuclear-explosion craters, large lunar primary craters (Shoemaker, 1965), and basins (Wilhelms and others, 1978) all slope between about −3.6 and −4.0. These slopes, which are much steeper than the −1.8 to −2 typical of primary craters, confirm the visual impression that secondaries in a given cluster are more nearly equal in size than are primaries in any given population. Over the entire size range, satellitic craters are concentrated at distances of one to two diameters from the primary's center (one to three radii from the rim crest; figs. 3.4, 3.8–3.10). Even the detailed map patterns of satellitic-crater fields of craters and basins are similar; chains, clusters, and loops are as characteristic of basin secondaries as they are of crater secondaries (Offield, 1971; Stuart-Alexander, 1971; Wilhelms and McCauley, 1971; Stuart-Alexander and Tabor, 1972; Scott, 1972b; Hodges, 1973a, b; Saunders and Wilhelms, 1974; Oberbeck and others, 1975; Schultz, 1976b, p. 276; Wilhelms, 1976; Ulrich and others, 1981, pl. 12). Patterns of ridges between and distal to clustered basin secondaries resemble those of crater secondaries and those formed in laboratory experiments (figs. 3.4, 3.7; Oberbeck and Morrison, 1973a, b, 1974, 1976; Oberbeck and others, 1975; Wilhelms, 1976). The only significant difference is a greater radiality of many basin-secondary groups; low impact velocities and grazing impacts create groovelike crater chains near basins (figs. 3.9*A*, 3.10*A*).

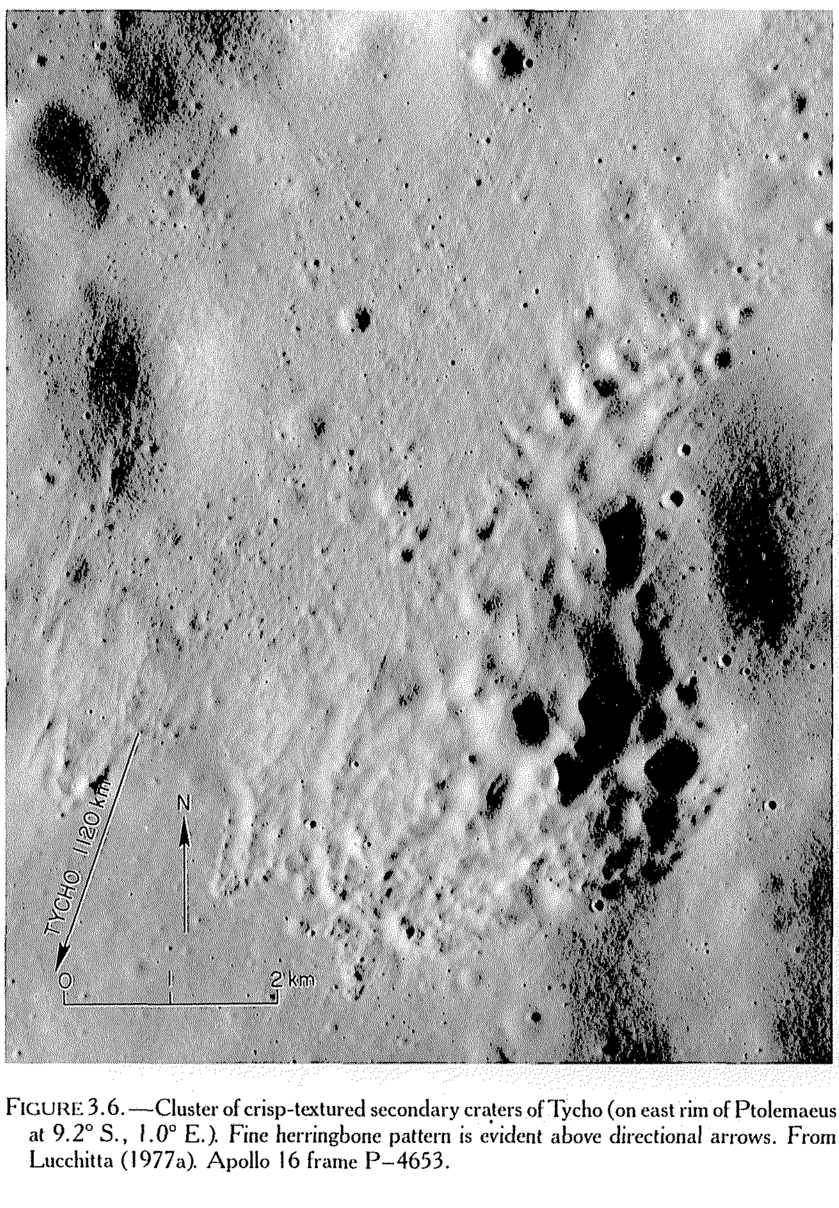

FIGURE 3.6.—Cluster of crisp-textured secondary craters of Tycho (on east rim of Ptolemaeus at 9.2° S., 1.0° E.). Fine herringbone pattern is evident above directional arrows. From Lucchitta (1977a). Apollo 16 frame P–4653.

The accumulated evidence on distribution and morphology (table 3.1) leaves little doubt that secondary craters compose a large percentage of lunar craters. They probably outnumber primaries at diameters smaller than 20 km and also occur with diameters of at least 30 km (Wilhelms and others, 1978).

Atypical craters

Continued research has expanded the types of morphology ascribable to impact. Although hypervelocity impacts normally create circular craters, impacts at angles less than 10° in weak materials or about 30° for certain combinations of target material, projectile material, and velocity may generate noncircular craters (Gault and Wedekind, 1978). Elongate craters, such as Messier and Schiller (fig. 3.11), have been interpreted as volcanic or volcanotectonic. However, craters formed by artificial oblique impacts mimic their shapes (figs. 3.12, 3.13; Moore, 1976; Gault and Wedekind, 1978). Ejecta symmetry in these experiments was typically bilateral; ejecta was concentrated in lateral or downtrajectory directions, as is the Messier ejecta (fig. 3.11*A*). The Messier ejecta possesses such typical impact characteristics as radial ridges, secondary craters, and rays. The position of Schiller along a basin ring (fig. 3.11*B*) was considered as supporting the endogenic interpretation (Offield, 1971; Schultz, 1976b, p. 20). Schiller, however, consists of overlapping elliptical craters that could have been created by oblique, nearly simultaneous impact of a fragmented projectile or by a very low-angle impact of the type simulated by Gault and Wedekind (top center, fig. 3.12).

Similarities of neighboring craters have long impressed scrutinizers of the lunar surface (for example, Baldwin, 1963, p. 189; see discussion by several observers in Hess and others, 1966, p. 308–309). Examples of pairs include Sabine and Ritter, Messier and Messier A, Heis and Caroline Herschel, Helicon and Le Verrier, and Atlas and Hercules (figs. 1.6, 1.7, 3.11*A*, 3.14). Some of these pairs may be accidental—Atlas and Hercules probably differ in age—but too many pairs exist to be entirely coincidental. Although endogeny was commonly invoked (for example, De Hon, 1971), diagnostic features show that an impact origin is more likely. Straight septa dividing some of these pairs (fig. 3.14*A*) had been considered evidence for a volcanic origin until they also were found at Henbury (Milton and Michel, 1965; Milton, 1968b) and among secondary-impact craters (Oberbeck, 1971b). Many of the craters are too large to be secondaries. Pairs of large impact craters, such as East and West Clearwater, Quebec, also occur on the Earth (for example, Dence, 1964, 1965; Oberbeck, 1971b).

Two primary-impact mechanisms have been proposed to explain the lunar groupings. First, Sekiguchi (1970) showed that tidal forces may break up weak approaching bodies before they impact. Second, small bodies may orbit mutually in space. The existence of these miniature planetary systems was surmised by Baldwin (1963, p. 21, 189) and may have been substantiated astronomically (for example, Binzel and Van Flandern, 1979).

Another atypical class of craters are those called smooth-rimmed (fig. 3.15; Wilhelms and McCauley, 1971). They lack the rough rim texture of main-sequence craters and have been considered to be of nonimpact origin. Apollo astronauts called them delta-rim craters because of their equal exterior and interior slopes—another departure from the main sequence, with its shallow outer and steeper inner slopes. They were targeted for special attention during the Apollo orbital missions because they were widely hypothesized to be calderas (El-Baz and others, 1972; Evans and El-Baz, 1973). Most smooth-rimmed craters are about 20 to 40 km across and occur near the borders of maria, a reasonable site for volcanism. The possible significance of smooth- rimmed craters was brought home when Lunar Orbiter 4 photographed two craters inside the Orientale basin that are, therefore, of the same maximum age (fig. 3.15*A*; McCauley, 1968). Maunder is a typical fresh impact crater, complete with high and rough inner rim, lower and radially textured outer rim flank, deep floor, rugged central peak, wall terraces, and secondary craters. The neighboring crater Kopff is opposite in each of these properties; it has a smooth "delta" rim, elevated floor, no peak or terraces, and no obvious secondary craters.

Although the smooth-rimmed craters are atypical, they also are probably of impact origin. A multivariate analysis of 11 pairs of dimensions of terrestrial and lunar craters shows that they group with impact craters (Pike, 1980c). Kopff may have been formed by an impact in a soft substrate (Wilhelms and McCauley, 1971; Guest and Greeley, 1977, p. 115, 153), or it may be merely a premare "hybrid" crater whose rim was smoothed by volcanism and whose floor was uplifted before and after mare flooding. Other smooth rims and elevated floors are consistent with similar modifications or with a secondary-impact origin (fig. 3.15). The more typical crater Maunder is simply younger than the smooth-rimmed craters and is not affected by either volcanism or floor uplift.

In summary, we are left with impacts as the generators of most lunar craters. Chapter 5 describes the relatively uncommon endogenic craters, and chapter 6 the modification of impact craters by floor uplift. With these relatively few exceptions and a few anomalous groups or individual craters (fig. 3.16), most features of lunar craters are compatible with current impact theory.

CRATERING MECHANICS

Introduction

The basic processes that form simple impact craters are now relatively well understood after two decades of intensive research on laboratory impact craters, explosion craters, and natural terrestrial and lunar craters. This section describes an idealized sequence of events based on studies of these relatively simple craters. It adds interpretations of complex craters and suggests some of the difficulties that confront investigators trying to understand craters and ringed basins more fully. The discussion draws heavily on earlier summary works by Shoemaker (1960, 1962b, 1963), Moore and others

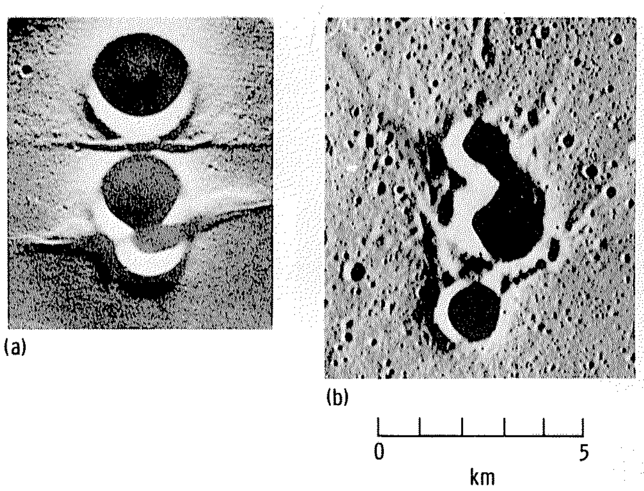

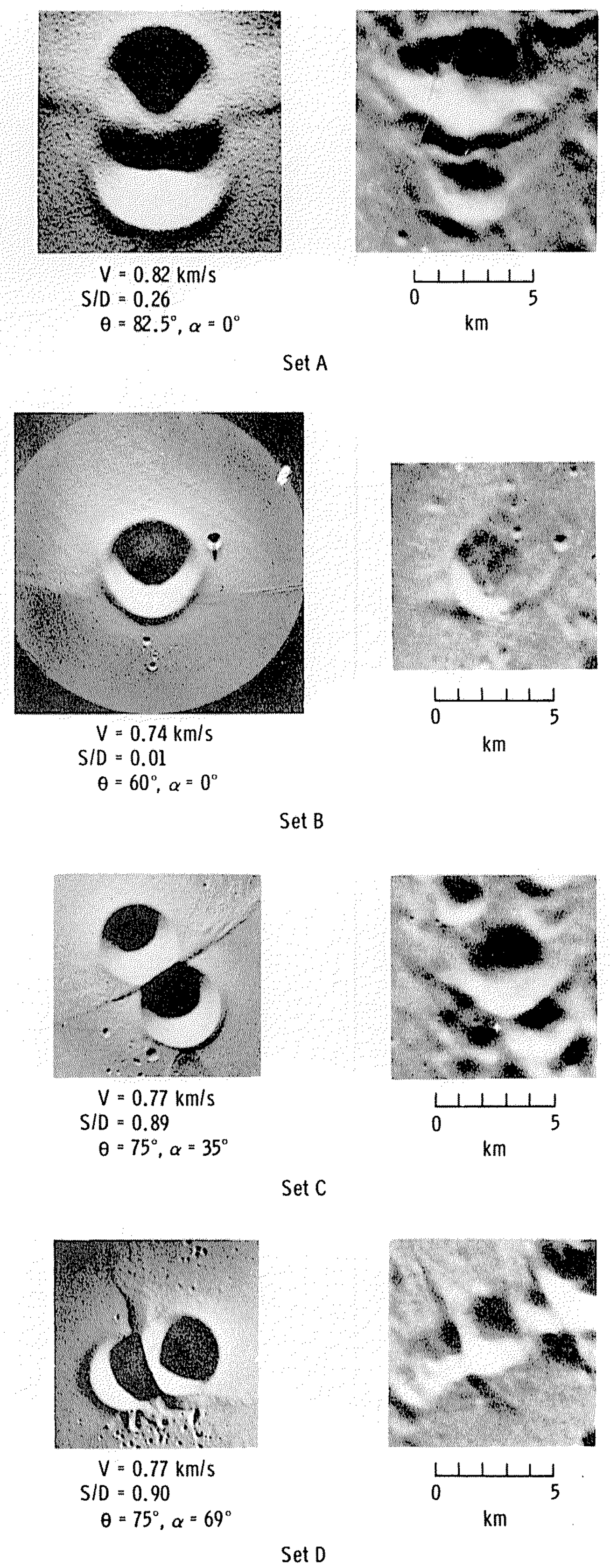

FIGURE 3.7.—Craters formed by near-simultaneous impacts in the laboratory, compared with morphologically similar secondary clusters of Copernicus (from Oberbeck and Morrison, 1973, p. 32–25). In each pair of examples, laboratory craters are on left, and lunar craters on right. *V*, experimental impact velocity; *S/D*, ratio of separation between impact points to average crater diameter; θ, impact angle of incidence measured from normal to surface; α, angle between crater axis of symmetry and flightline or radial line from Copernicus. Projectiles impacted from direction below photographs. Lunar photographs, Apollo 15 frame M-1699 (upper left) and Orbiter 4 frame H–121 (all others) (compare fig. 3.4C).

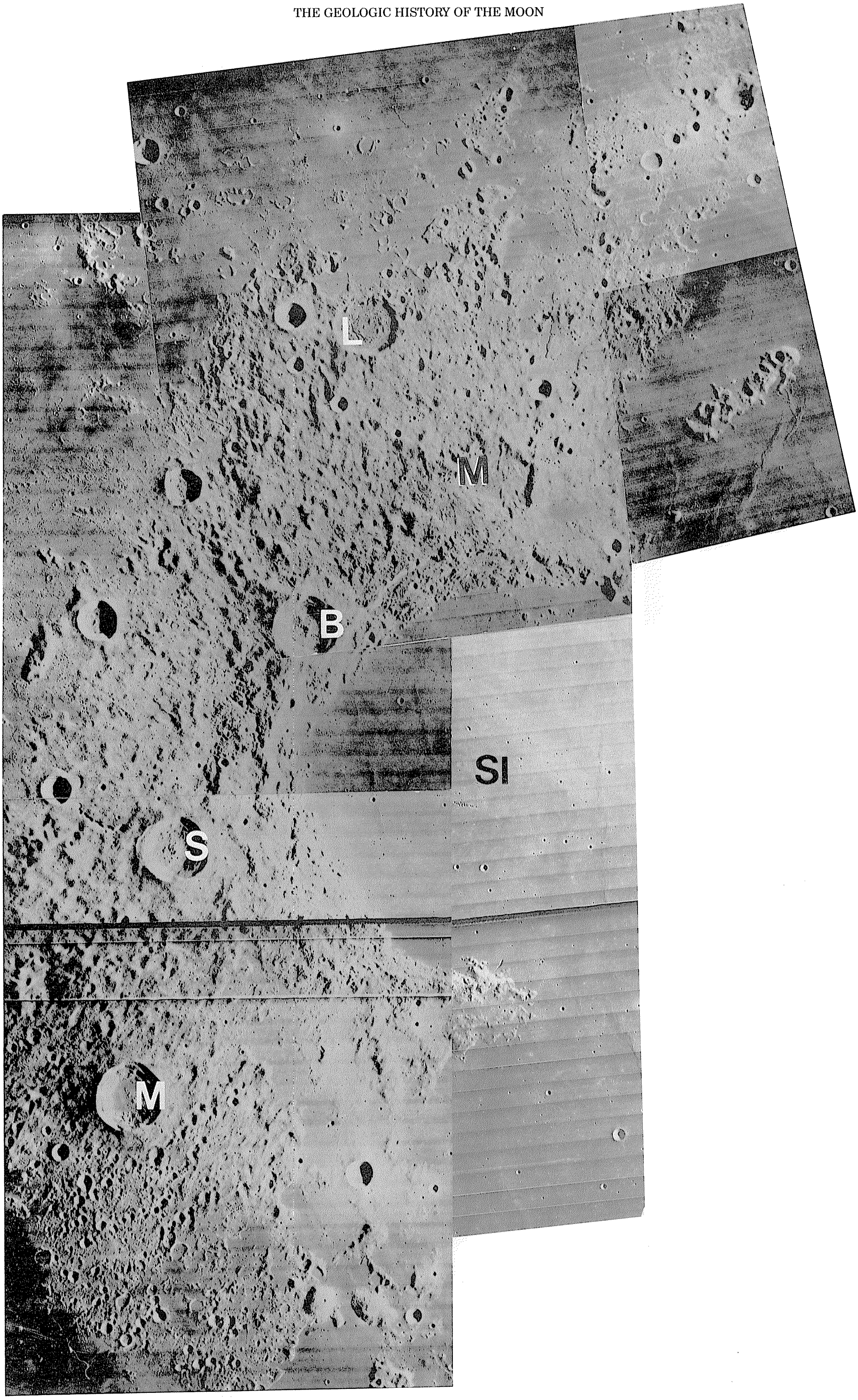
L
M
B
SI
S
M

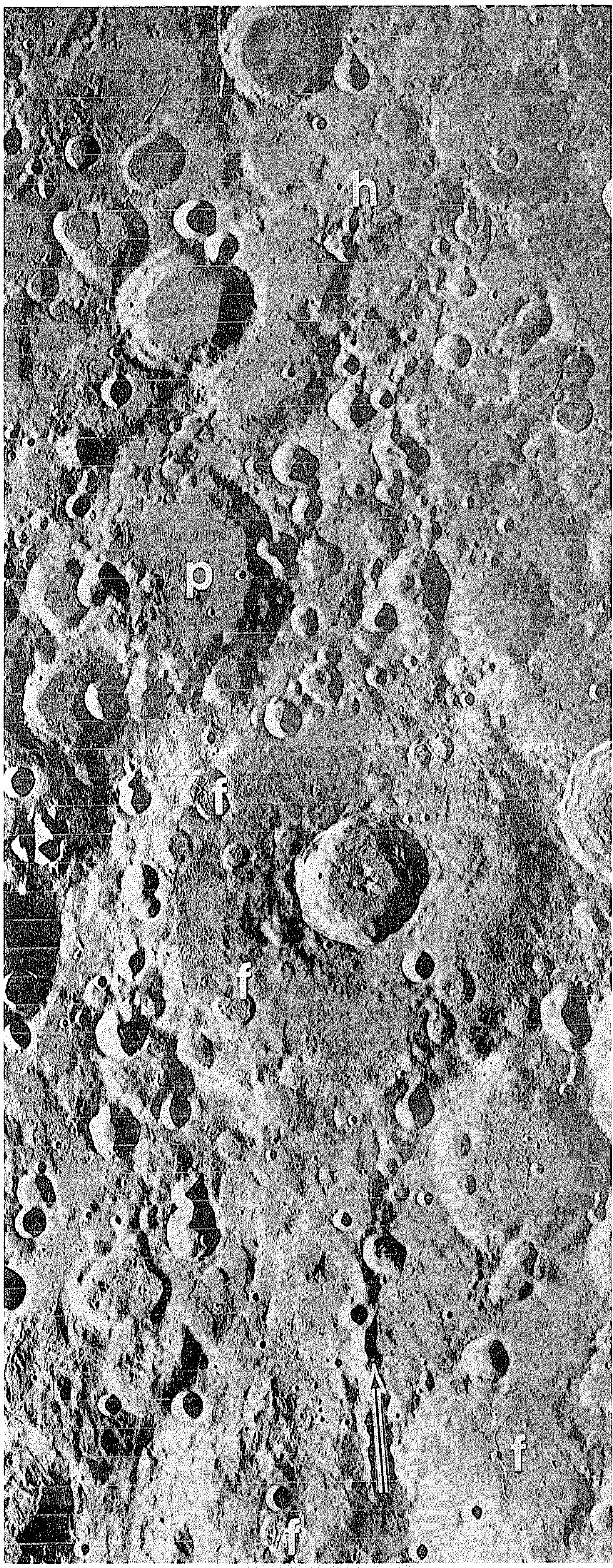

A

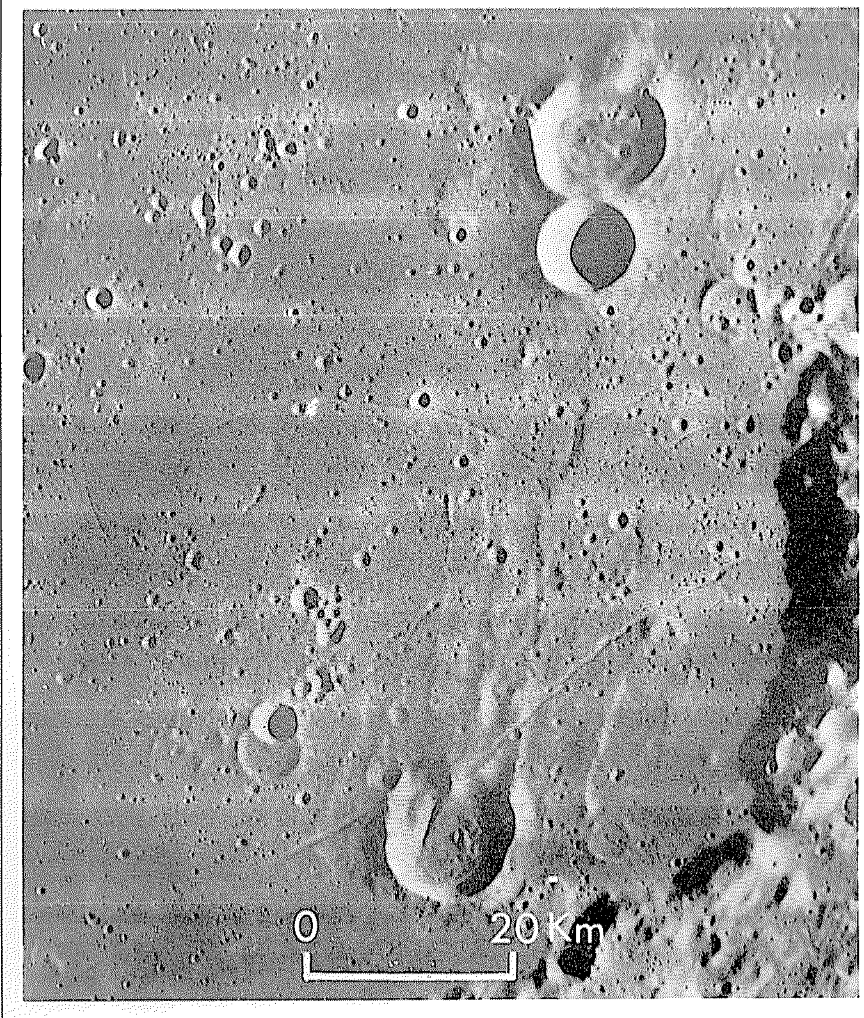

B

FIGURE 3.9.—Diverse Orientale-basin secondary craters north of the basin.

A. Chain (Vallis Bohr, arrow at bottom), clustered circular craters, fissured crater floors (f), and herringbone pattern (h, near top), all formed by impact of Orientale ejecta. Head of arrow marks one basin diameter (930 km) from basin center (one radius from rim). Thick ejecta plains form scarp at p (see chap. 4). Large crater occupying most of photograph width is Einstein (170 km, 17° N., 88.5° W.). Orbiter 4 frame H–188.

B. Domelike interference feature and radial ejecta of crater Struve L (above scale bar; 15 km, 21° N., 76° W.), 1,350 km north-northeast of Orientale center. Orbiter 4 frame H–174.

FIGURE 3.8.—Iridum crater (260 km; compare fig. 1.6) enclosing Sinus Iridum (SI). Almost entire terra in scene is blanketed by Iridum deposits or secondary craters; secondaries appear at about one radius from rim of Iridum crater. Superposed craters are Bianchini (B; 38 km), Mairan (white M; 40 km, 42° N., 43° W.), and Sharp (S; 40 km); pre-Iridum craters are La Condamine (L; 37 km, 53° N., 28° W.) and Maupertuis (black M; 46 km). Mosaic of Orbiter 4 frames H–139, H–145, and H–151 (from right to left).

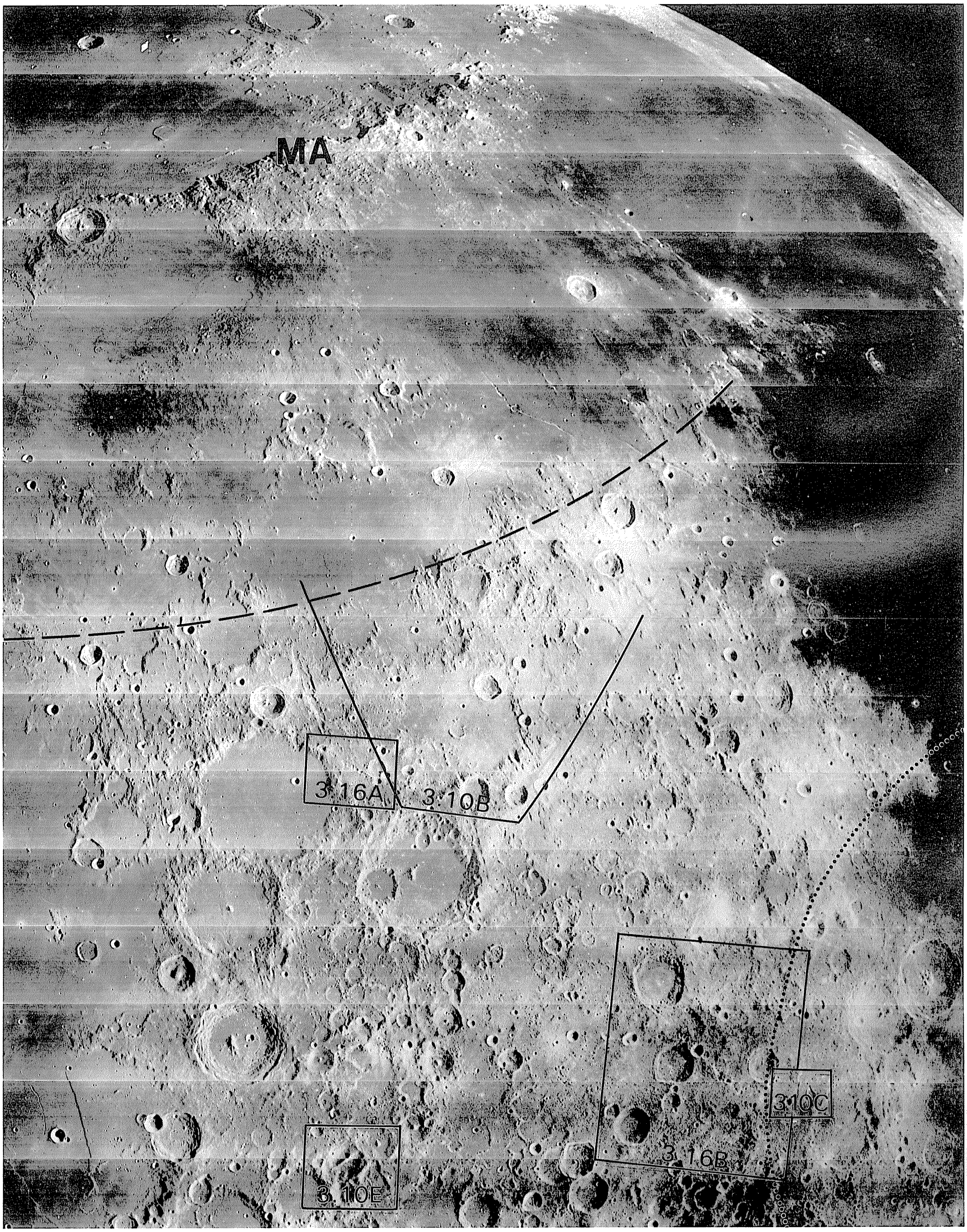

FIGURE 3.10.—Secondary craters of Imbrium and Nectaris basins.

A. Regional view, showing distance of one basin radius (dashes, 580 km) from Imbrium rim (MA, Montes Apenninus); dotted outline, Nectaris rim. Locations of figures 3.10*B*, *C*, *E* and 3.16*A*, *B* are outlined; figure 3.10*D* lies below area of photograph. Orbiter 4 frame M–108.

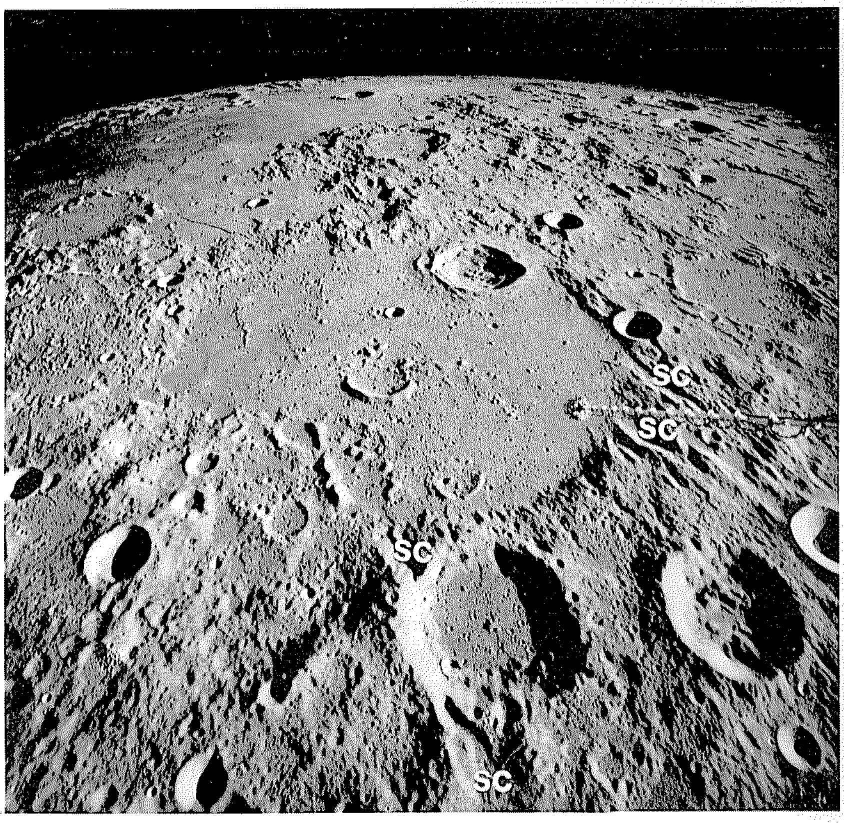

B

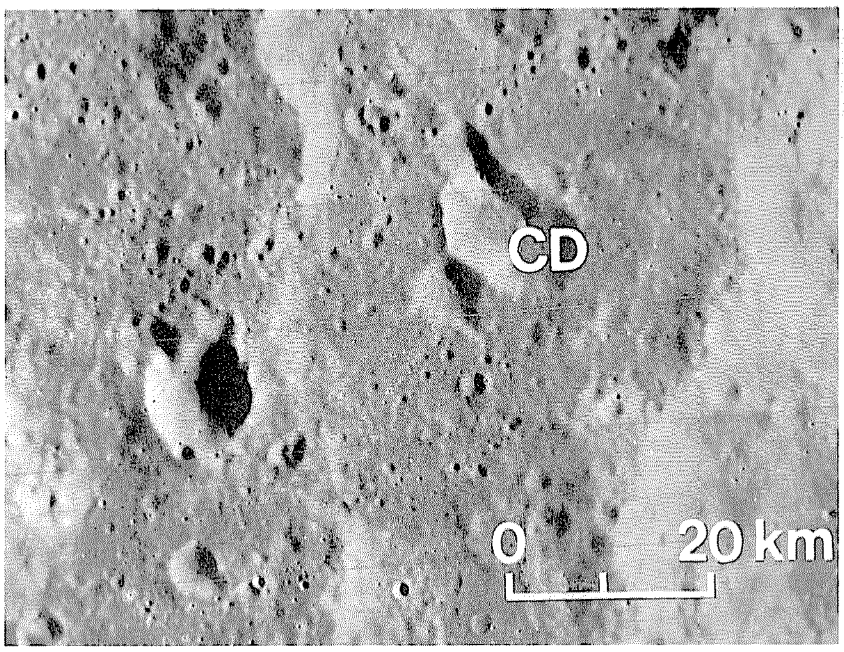

C

B. "Imbrium sculpture," evidently composed of coalescing elliptical craters (sc). Large crater is Hipparchus (151 km, 6° S., 5° E.). Gamma-ray spectrometer boom protrudes from right. Apollo 16 frame M–839.

C. Crater Catharina D (CD; 9 km, 19° S., 21° E.) has been considered volcanic (Wilhelms and McCauley, 1971), but is oriented and situated properly (fig. 3.10*A*) to be an Imbrium-basin secondary. Orbiter 4 frame H–84.

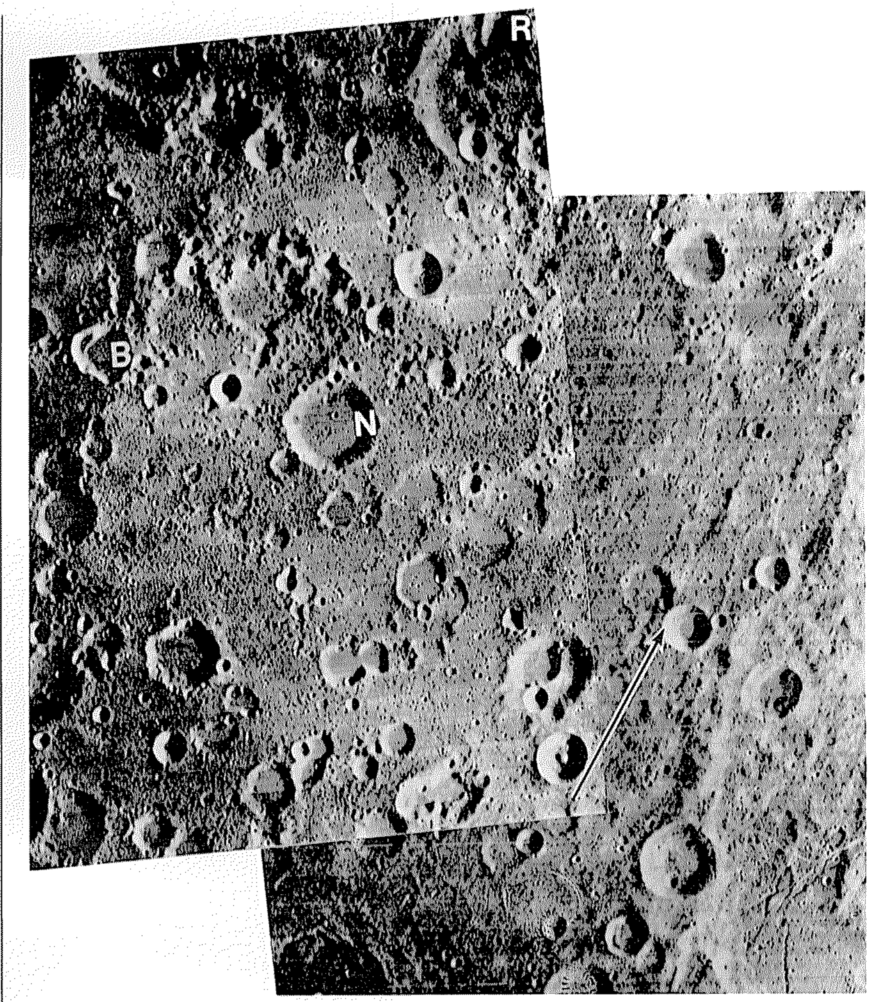

D

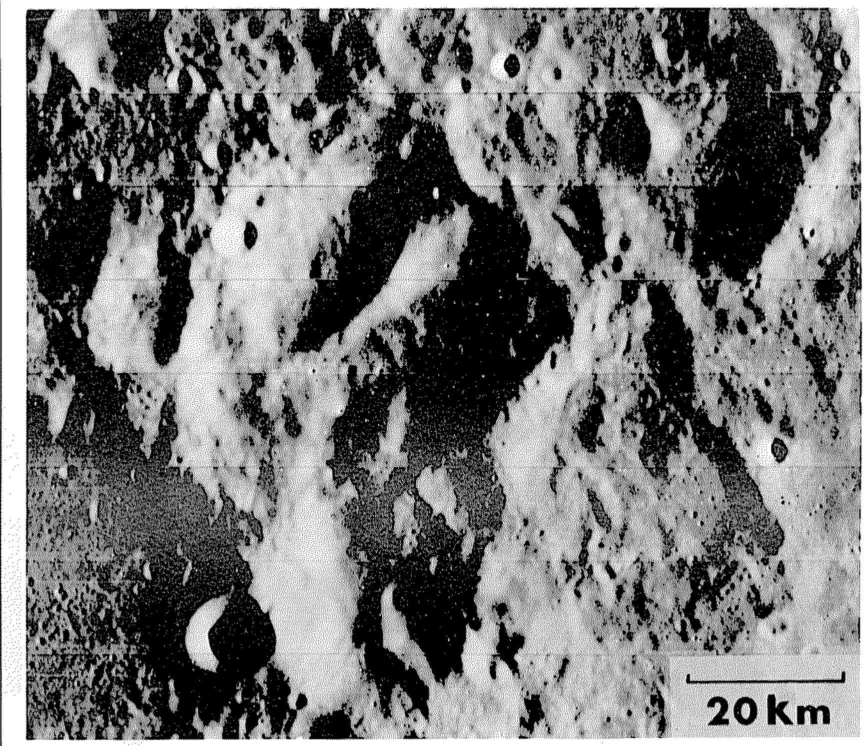

E

D. S-shaped group of Imbrium secondaries looping southward from rim of crater Riccius (R; 71 km, 37° S., 27° E.) to crater Nicolai (N; 42 km, 42° S., 26° E.) and back toward basin in another loop ending at crater Barocius G (B; 27 km). Arrow indicates direction to Nectaris basin; partly filled craters south of (below) Nicolai and west (left) of arrow are probably secondaries of Nectaris. Large crater Janssen (190 km; compare fig. 9.2) is partly visible in lower right. Orbiter 4 frames H–83 (right) and H–88 (left).

E. Complex morphology of Delaunay group of craters, suggesting volcanism or interference of several large basin-secondary craters (Holt, 1974). View centered at 22.5° S., 3° E. Orbiter 4 frame H–101.

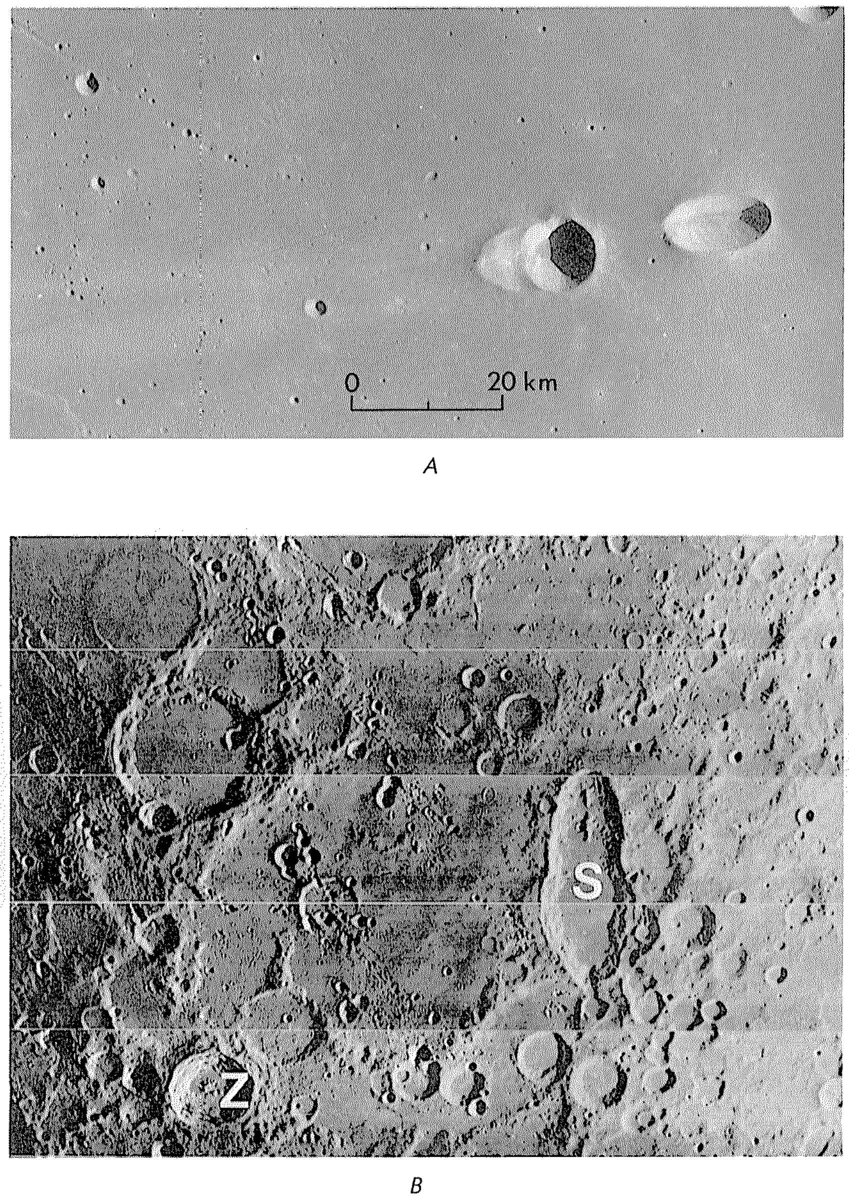

FIGURE 3.11.—Irregular primary-impact craters.

A. Messier (right) and Messier A (2° S., 47° E.). Radial ejecta and rays are north and south of Messier, and long double rays to west (down trajectory). Apollo H-frame (number unknown).

B. Schiller (S, footprint-shaped crater; 180-km long axis), superposed on ring of double-ringed Schiller-Zucchius basin (compare fig. 1.9); Z, crater Zucchius (64 km, 61° S., 50° W.). Orbiter 4 frame M–155.

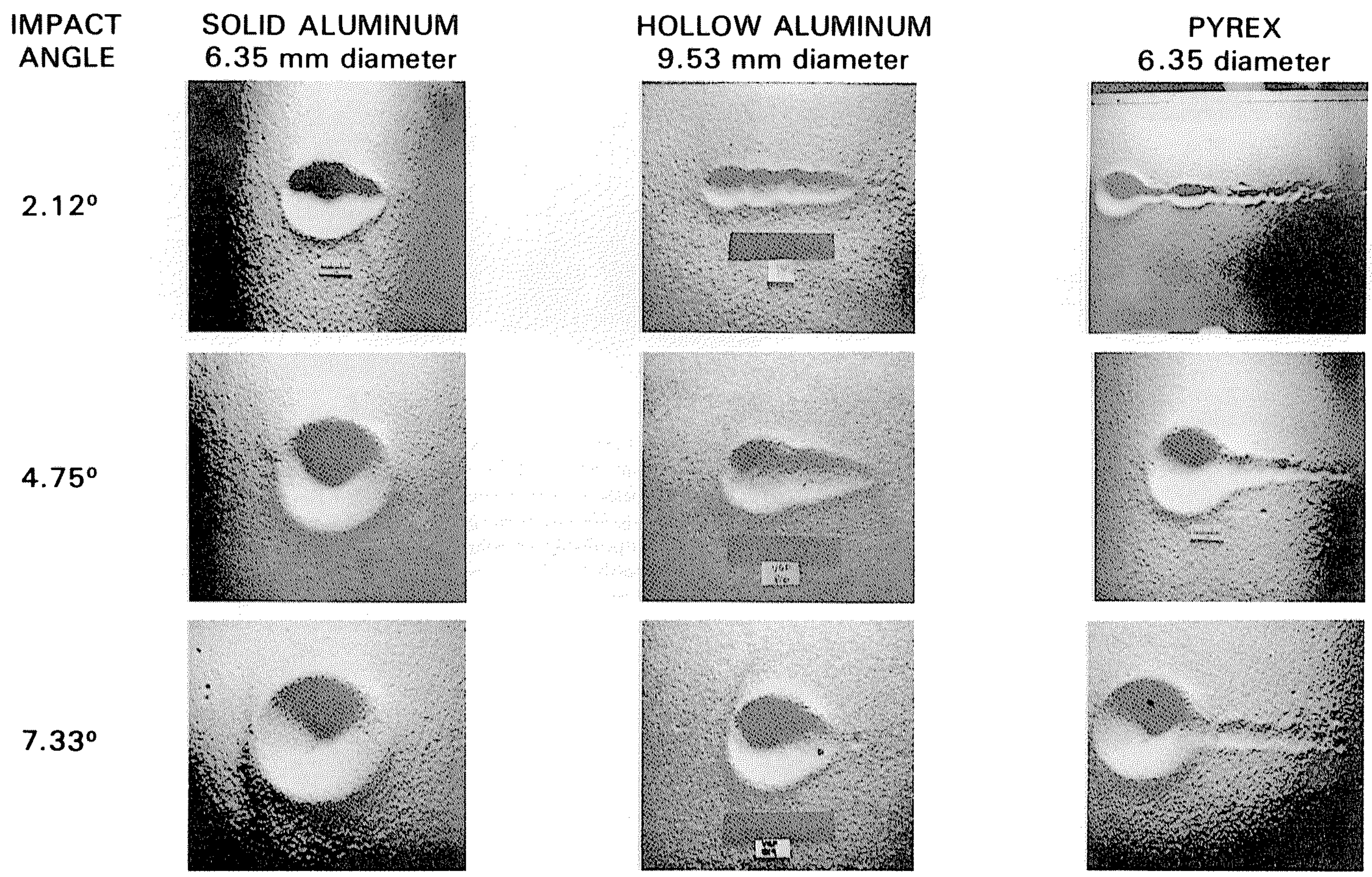

FIGURE 3.12.—Craters formed by oblique impacts in laboratory (from Gault and Wedekind, 1978, fig. 4). Spherical projectiles are described at top; target is noncohesive quartz sand. Impact velocity, about 1.7 km/s; impact angles, above plane of target surface; trajectories, from left.

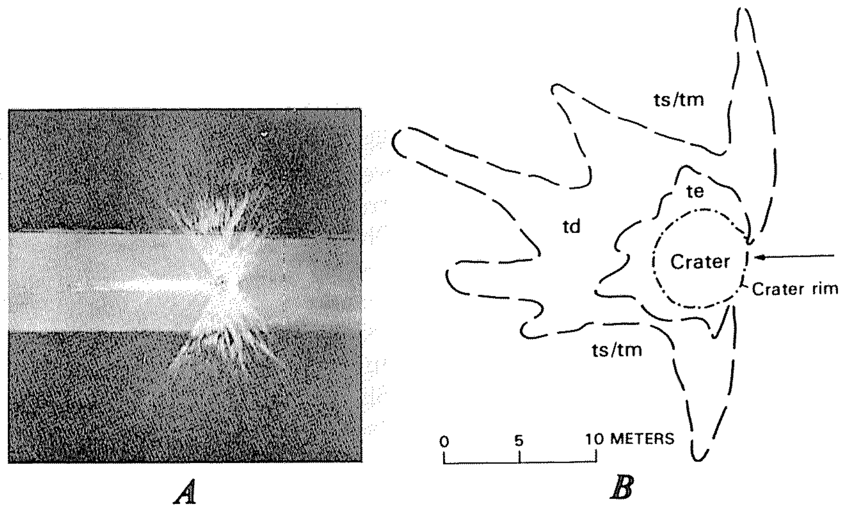

FIGURE 3.13.—Ray patterns formed by oblique impacts (from right).
A. In laboratory (Gault and Wedekind, 1978, p. 3855). Impact angle, 5° above horizontal.
B. By ballistic missile at White Sands Missile Range, N. Mex. (Moore, 1976, p. B8). Material units: te, thick ejecta; td, thin to discontinuous ejecta; ts/tm, scattered ejecta and target material. Arrow indicates missile trajectory; impact angle, about 45°.

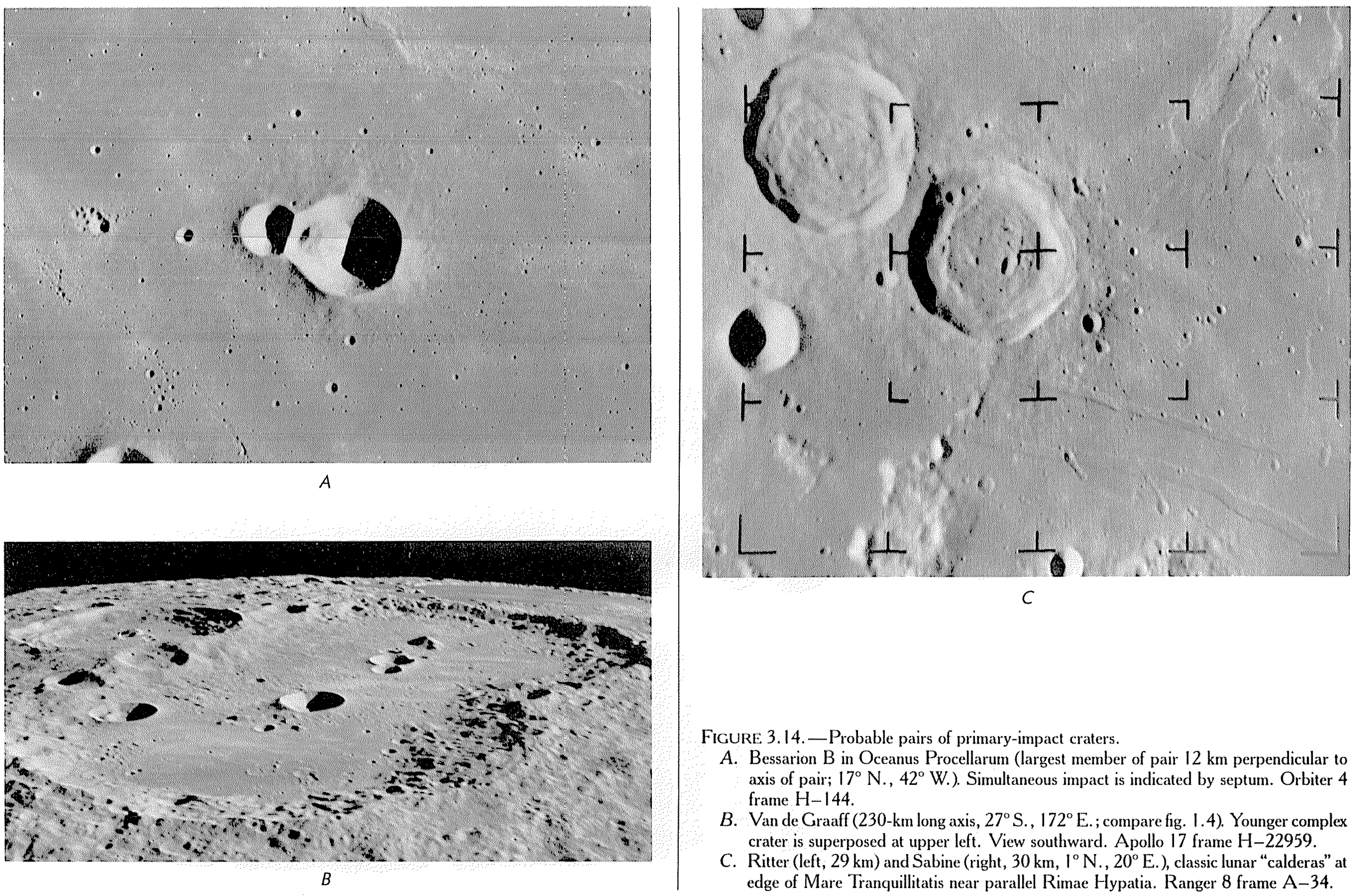

FIGURE 3.14.—Probable pairs of primary-impact craters.
A. Bessarion B in Oceanus Procellarum (largest member of pair 12 km perpendicular to axis of pair; 17° N., 42° W.). Simultaneous impact is indicated by septum. Orbiter 4 frame H–144.
B. Van de Graaff (230-km long axis, 27° S., 172° E.; compare fig. 1.4). Younger complex crater is superposed at upper left. View southward. Apollo 17 frame H–22959.
C. Ritter (left, 29 km) and Sabine (right, 30 km, 1° N., 20° E.), classic lunar "calderas" at edge of Mare Tranquillitatis near parallel Rimae Hypatia. Ranger 8 frame A–34.

(1961), Baldwin (1963), Gault and others (1968b), Gault (1974), Oberbeck (1975), Roddy and others (1977), and Melosh (1980). Much of the material in the volume edited by Roddy and others (1977) was summarized by Cooper (1977).

Shock compression

An impact crater results from the meeting of an irresistible force with an immovable object (Baldwin, 1963, p. 6). A hypervelocity collision generates intense high-pressure shock waves that propagate into both the target and the projectile (Shoemaker, 1960, 1962b; Melosh, 1980). As the shock front moves downward and outward into the target, masses are set into motion with particle velocities much greater than the speed of sound in the various materials. Pressures and energies within the shock wave are commonly so great that parts of both the target and projectile are melted and vaporized around the impact zone (Gault and Heitowit, 1963). More significantly for the ultimate crater, the shock wave strongly compresses and energizes a mass of target material much greater than that of the projectile (Shoemaker, 1962b, p. 317; Gault and others, 1968b). Because peak pressures in the shock wave are orders of magnitude above the strengths of all rock materials, the materials flow hydrodynamically (Shoemaker, 1960; Gault and others, 1968b; Dence and others, 1977; Roddy, 1977). In homogeneous targets, shock waves propagate outward in approximately spherical fronts (fig. 3.17; Gault and others, 1968b). The pressures in the shock wave quickly diminish radially outward, until eventually the shock wave decays into an elastic wave (Shoemaker, 1960). The distance at which the shock wave becomes elastic is a function of original kinetic energy, projectile penetration depth, duration of contact, rock properties, and deflections due to layering and other inhomogeneities (Shoemaker, 1962b, p. 320).

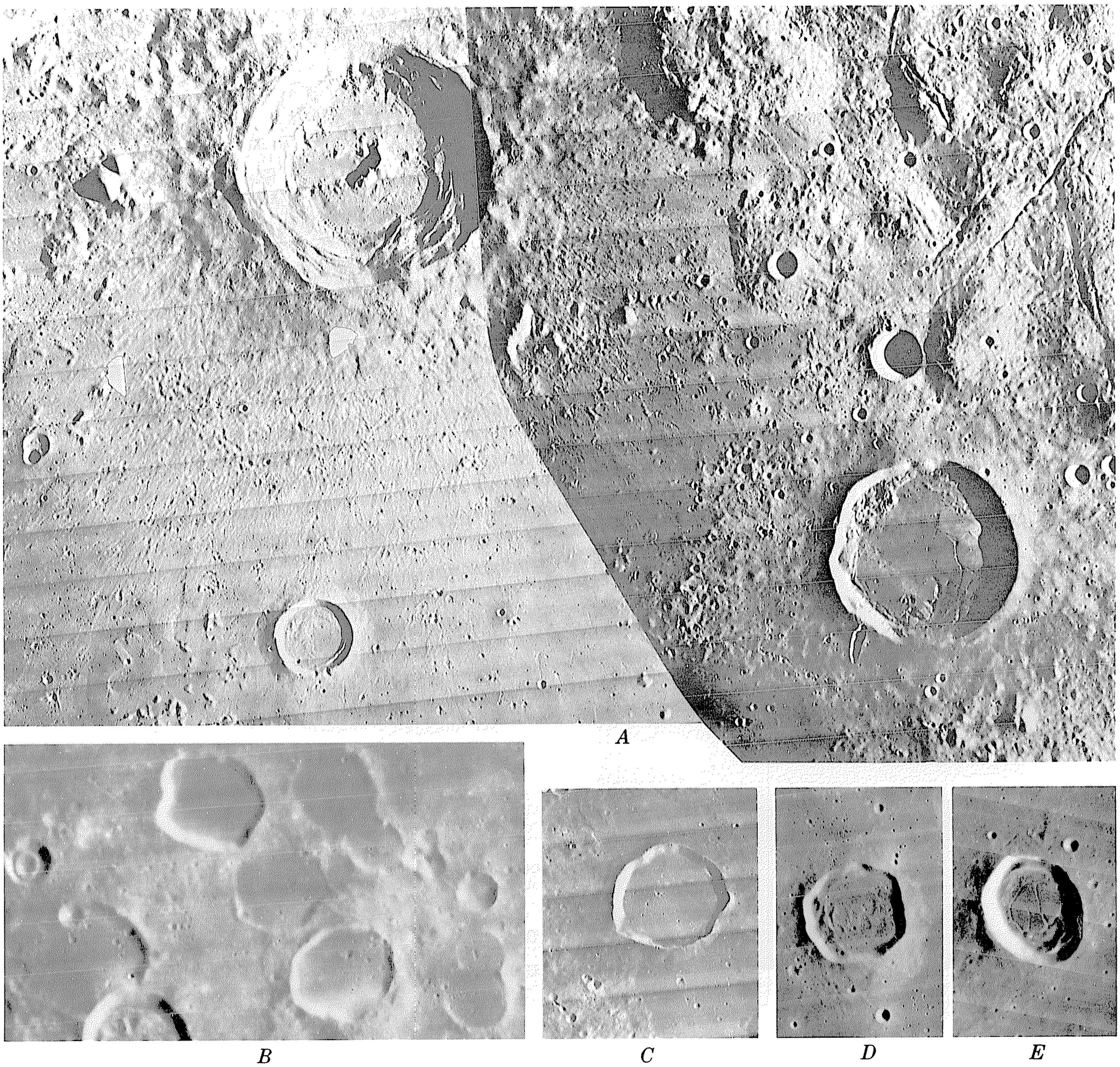

FIGURE 3.15.—Smooth-rimmed class of craters (Wilhelms and McCauley, 1971).

A. Contrasting craters in Orientale basin: Kopff, right (42 km, 17° S., 89.5° W.), a smooth-rimmed crater; Maunder, left (55 km, 15° S., 94° W.), a typical impact crater. Orbiter 4 frames H–187 (right) and H–195 (left).

B. Crozier-McClure group on Fecunditatis-basin rim (14° S., 51° E; each of three central craters, 21–24 km across). Clustering and smooth rims suggested caldera origin (Wilhelms and McCauley, 1971), but radial orientation and size range are also consistent with Imbrium-secondary origin. Orbiter 4 frame H–60.

C. Gambart (25 km, 1° N., 15° W.). Dark rim material is probably volcanic, but current interpretations favor superposed pyroclastic material rather than volcanic ejecta of crater. Orbiter 4 frame H–120.

D. Lassell (23 km, 15.5° S., 8° W.) in eastern Mare Nubium. Orbiter 4 frame H–113.

E. Daniell (29 km, 35° N., 31° E.) in Lacus Somniorum. Volcanic origin is suggested, but not proved, by irregular rim crest, elevated floor, and mare fill. Orbiter 4 frame H–79.

Cavity excavation and growth

Very early in the sequence of events, even before the shock wave reaches the projectile's trailing edge, small amounts of both the projectile and target material may be jetted from the sides of the impact zone at velocities that may exceed the initial velocity of the projectile (fig. 3.17*A*; Gault and others, 1963, 1968b; Kieffer and Simonds, 1980). Most ejection, however, takes place at velocities first comparable to and then much lower than the initial projectile velocity. The agents of excavation in this main cratering-flow stage of ejection and cavity growth are rarefactions set up when the shock wave intersects the free surfaces and other discontinuities in the target and projectile. The result is a sudden decompression. Particles of material are deflected from the initially radial motions induced by the shock wave into upward and outward trajectories curving back toward the surface on the heels of the expanding shock wave (figs. 3.17*B–E*; Shoemaker, 1960, 1962b, p. 320; Gault and others, 1968b; Cooper, 1977, p. 37–38; Grieve and others, 1977, p. 801–804; Kreyenhagen and Schuster, 1977; Roddy, 1977, p. 297; Trulio, 1977; Melosh, 1980). Thus, most impact-crater excavation is a response to the disequilibrium suddenly induced by the intensely energetic, penetrative shock wave and is not the direct result of an expansion like that induced by a true chemical explosion (Shoemaker, 1962b, p. 316). Another difference from most explosions is that the energy from a hypervelocity impact is released along the length of the path of penetration, which may be short or may be an elongate, cigar-shaped zone (Jones and Sandford, 1977, p. 1009; Gault and Wedekind, 1978). Explosions at moderately shallow depths, however, may mimic impact effects (Shoemaker, 1960, 1963; Baldwin, 1963, chap. 7; Roddy, 1968, 1977; Oberbeck, 1971a, 1977; Melosh, 1980) because their energy may be coupled into the ground similarly (Cooper and Sauer, 1977; Knowles and Brode, 1977, p. 874; Kreyenhagen and Schuster, 1977; Trulio, 1977).

Because the decompression and not the direct, intense shock compression excavates most of the cavity, ejection endures longer than the shock compression (Gault and others, 1968b). After most of the projectile material has been ejected, the cavity, lined with partly molten material, continues to grow behind the advancing shock wave by ejection of target material (figs. 3.17*E*, *F*). Though basically orderly, at least in simple craters (Shoemaker, 1960; Gault and others, 1968b), the ejection process is more subject to vagaries stemming from inhomogeneous properties and structures of the target than is the shock-compression phase. For example, inhomogeneities are the probable cause of the pattern of secondary chains and loops (Shoemaker, 1962b).

Ejection of the target material occurs approximately in the order it is enveloped by the shock wave (Stöffler and others, 1975). In general, more highly shocked materials high in the target and just outside the impact zone leave first at the highest velocities and angles (measured above the horizontal). Molten material may be shot into high ballistic trajectories. Subsequently, expanding concentric zones that include more moderately shocked materials from increasingly deep target materials are successively ejected. The ejecta forms an upward- and outward-flaring curtain of debris in the shape of an inverted lampshade (a frustum). The materials that form this curtain are sheared up along the walls of the growing cavity to the cavity lip, where they leave at angles parallel to the walls (Gault and others, 1968b; Oberbeck, 1977, p. 46; Orphal, 1977); the curtain is like an extension of the crater wall. The curtain continuously expands outward during crater growth. It apparently always remains thin, at least in small craters (fig. 3.17; Oberbeck, 1975; Oberbeck and Morrison, 1976). Typical ejection angles for the main, middle stages of experimental crater formation are 40° to 60° above horizontal but also depart from these values, depending on such properties of the target material as layering and competence (Andrews, 1977; Orphal, 1977; Wisotski, 1977).

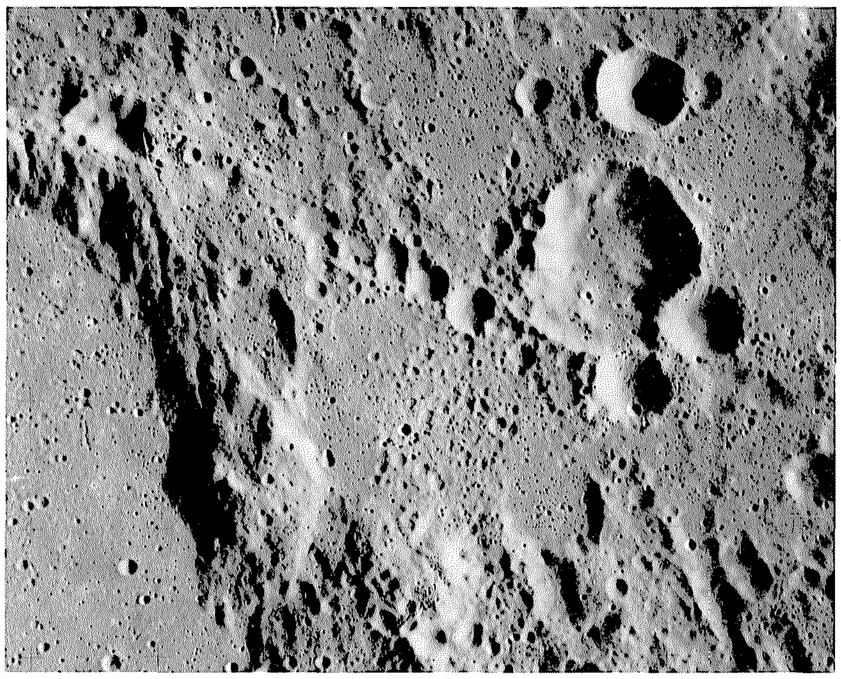

A

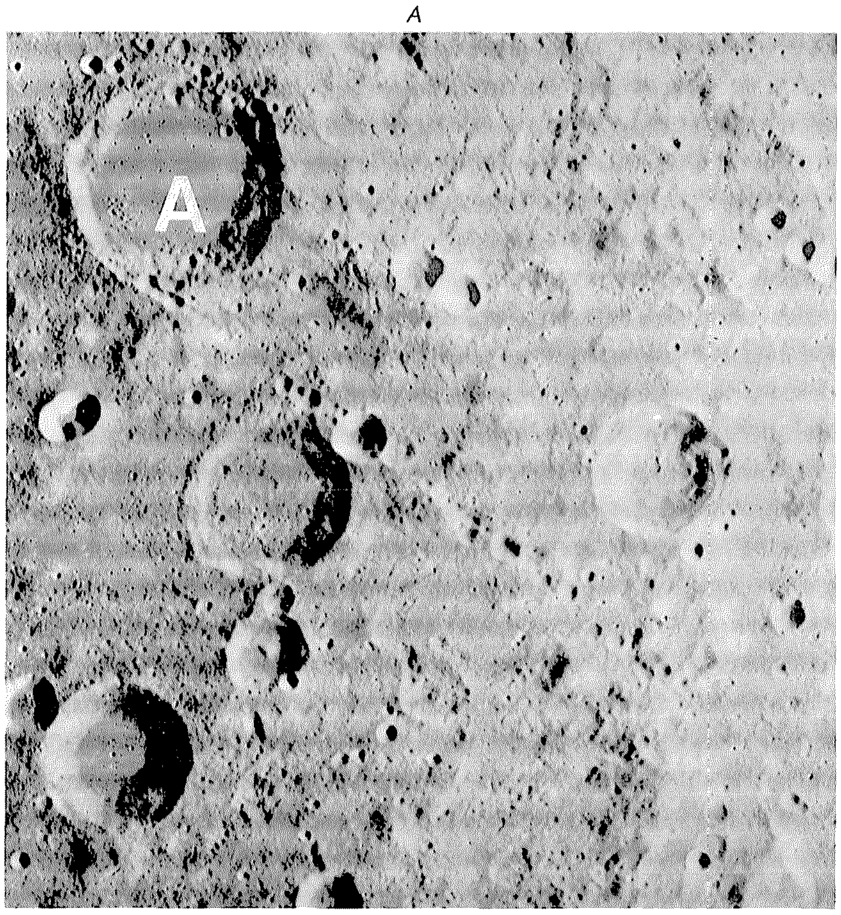

B

FIGURE 3.16.—Craters of undetermined origin (see fig. 3.10*A* for locations).

A. Müller group on east of rim of Ptolemaeus; largest crater is Müller (22 km, 8° S., 2° E.). Large craters exhibit morphology, size, and distal overlap typical of Imbrium-secondary craters at this radial distance (800 km from Montes Apenninus); "Imbrium sculpture" above and below chain is radial to Imbrium. Small chain is also typical of secondaries in morphology and overlap but is not radial to Imbrium or any other likely source. Apollo 16 frame M–1671.

B. Abulfeda chain, parallel to Müller chain and also site of numerous craters. A, Abulfeda (65 km, 14° S., 14° E.). Orbiter 4 frame H–89.

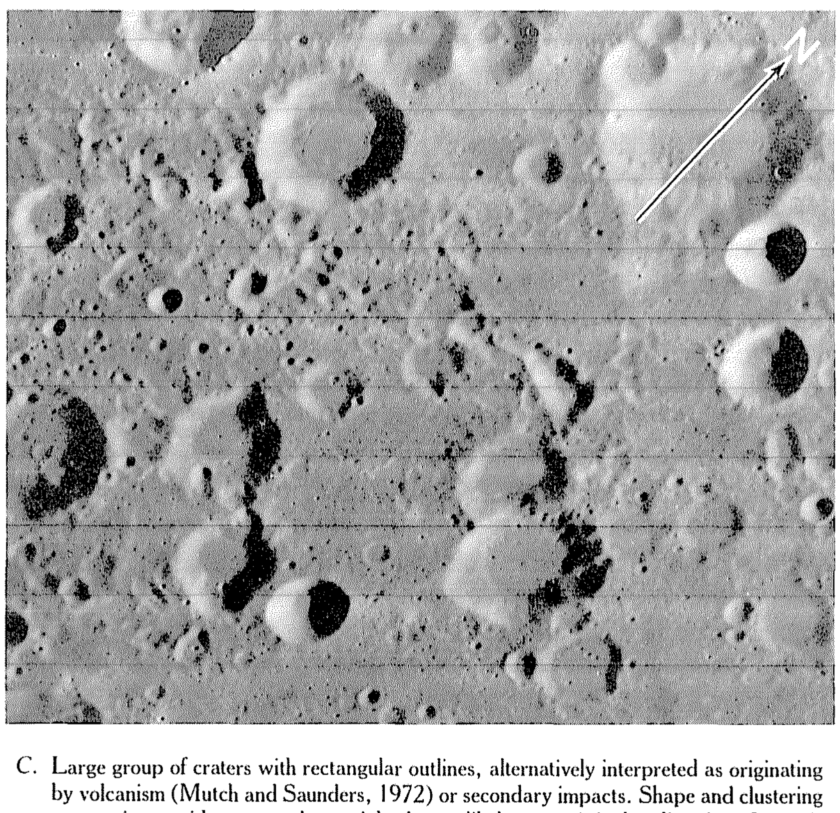

C. Large group of craters with rectangular outlines, alternatively interpreted as originating by volcanism (Mutch and Saunders, 1972) or secondary impacts. Shape and clustering are consistent with source to lower right, but no likely source is in that direction. Group is radial to Orientale basin, but Orientale secondaries at this distance are generally sharper (compare fig. 4.6). Several other large craters are also clustered and may be basin secondaries (Schultz, 1976b, p. 276). Crater under north arrow is Asclepi (43 km, 55° S., 25° E.). Orbiter 4 frame H–100.

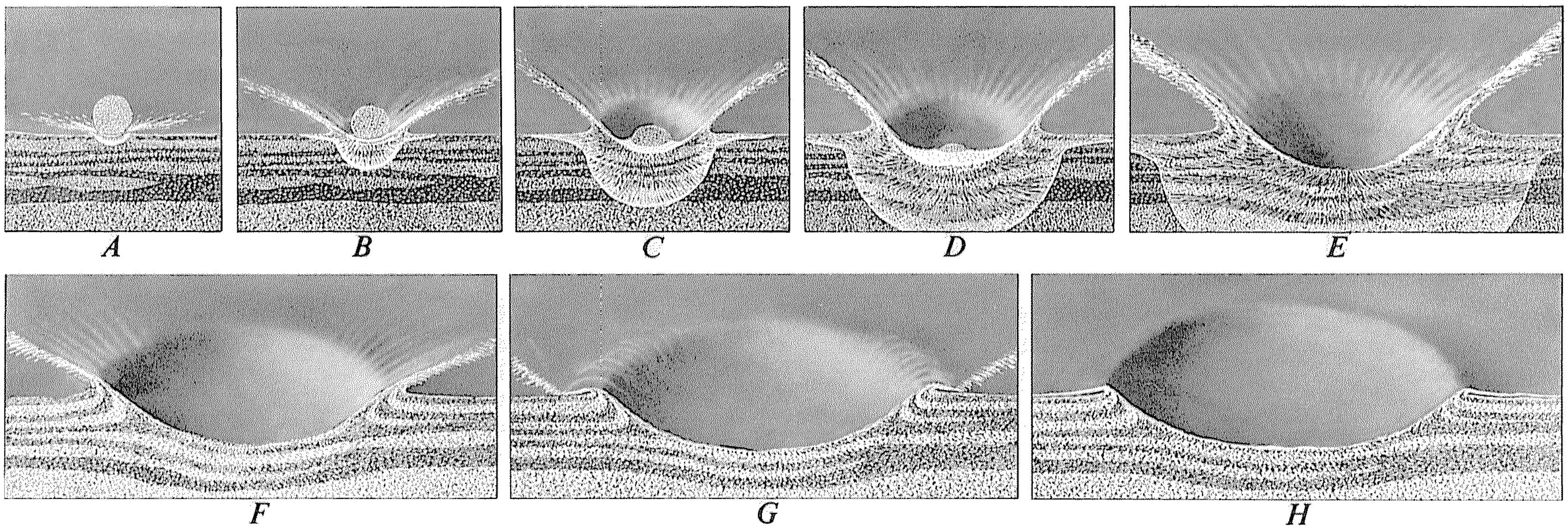

FIGURE 3.17.—Stages in formation of a simple impact crater. Drawing by Donald E. Davis, courtesy of the artist.
A. Initial contact and jetting.
B, *C*, *D*. Compressional shock wave propagates outward, and cavity grows by rarefaction behind shock wave while projectile is consumed.
E. Cavity continues growth after projectile has been consumed.
F. Maximum crater size.
G. Frustum-shaped curtain of ejected debris continues outward expansion after cavity ceases growth and overturned ejecta flap comes to rest.
H. Final crater configuration.

The cavity of a typical small simple crater ceases to expand downward when it has acquired depths of ⅕ to ½ of the diameter (Dence and others, 1977, p. 250–253; Knowles and Brode, 1977, p. 890–891; Orphal, 1977, p. 909). Shearing flow at the walls may then continue to broaden the crater after this maximum depth is reached (Orphal, 1977; Piekutowski, 1977; Swift, 1977). Weakly shocked and nearly undamaged ejecta derived from near the walls leaves last, during the final stages of crater excavation, under relatively low stresses and at low velocities and ejection angles (Shoemaker, 1962b, p. 335; Oberbeck, 1975; Stöffler and others, 1975; Andrews, 1977; Cooper, 1977, p. 25; Orphal, 1977). The size of ejected debris increases during cavity growth owing to decreasing shock pressures, decreasing fragmentation of the wallrock, and lower ejection velocities. Finally, ejection ceases as the tensile strength of the rock overcomes the power of the rarefaction wave to move it.

Ejecta deposition

After the cavity ceases to grow, the inverted frustum-shaped ejecta curtain continues to advance outward beyond the cavity (fig. 3.17*G*). The curtain continuously decreases in height while expanding in diameter, as materials at the base are deposited on the surface from the cavity rim outward. Because most ejecta is launched from a simple crater at nearly constant exit angles but at decreasing velocities, the ejecta front slopes outward at a nearly constant angle with the surface, generally 40°–50° (Oberbeck, 1975, 1977; Oberbeck and Morrison, 1976; Andrews, 1977, p. 1090–1092; Cooper, 1977, p. 38–39). As a result of this velocity distribution in the curtain, ejecta deposition occurs in approximately the reverse order of excavation. The first material to be deposited, from the base of the ejecta curtain, is the last to have been engulfed by the shock wave and to be sheared from the crater walls (figs. 3.17, 3.18). That material is lofted or barely pushed over the rim at low velocities and soon lands near the crater rim. In simple craters, the near-rim material may form a more or less coherent overturned flap in which the stratigraphic sequence of redeposited target materials is the reverse of their preimpact sequence (fig. 3.17*H*; Shoemaker, 1960, 1962b, 1963; Roberts, 1966; Roddy, 1968, 1976, 1977, p. 201; Stöffler and others, 1975; Moore, 1976; Oberbeck and Morrison, 1976). Some of the relief on crater rims is also due to structural upthrust and outthrust in a manner dependent on target structure and depth of energy release (Shoemaker, 1960, 1963; Roberts, 1968; Gault and others, 1968b). For a considerable time after the cavity stops growing, the curtain continues to move outward and to drop material from its lower edge into an ever-expanding but thinning ring of deposits.

Secondary cratering and ground surge

With increasing distance from the crater, the ejecta that strikes the surface forms secondary craters rather than building up a deposit. At some distance, the curtain separates into filaments of debris, whose impact creates loops and chains of secondary craters and rays. Circular secondaries are formed by the last material to impact the surface, that which was launched first at the highest velocities and in the longest, highest trajectories from sources high in the target near the impact zone.

The general picture, then, around craters as well as ringed basins is one of outward-thinning deposits of primary ejecta grading into increasingly conspicuous secondary craters and their ejecta deposits (Shoemaker and Hackman, 1962; Schmitt and others, 1967; Ulrich, 1969; Guest, 1973). The secondary impacts excavate material of the local terrain around the primary crater (Moore and others, 1974; Oberbeck and others, 1974, 1975, 1977; Morrison and Oberbeck, 1975, 1978; Oberbeck, 1975, 1977; Oberbeck and Morrison, 1976; Hörz, 1981). The amount of local material excavated increases outward. The picture is complicated around many craters and, particularly, around basins by the superposition on secondary craters of material that has flowed from points closer to the crater or basin (Shoemaker and Hackman, 1962, p. 291; Hodges, 1973b; Scott and Eggleton, 1973; Moore and others, 1974; Morrison and Oberbeck, 1975; Wilhelms, 1976, 1980). In the picture above of the regular advance of ejecta in a narrow curtain, the ejecta that forms the secondaries was still in flight when the ground-flow deposits left the crater, but the flying ejecta impacts the surface before the ground-flow deposits reach the secondary-impact zone.

The question of how the ground flow originates has been much debated because of its importance in studies of lunar-sample provenance. Chao (1974, 1977) and Chao and Minkin (1977) cited evidence

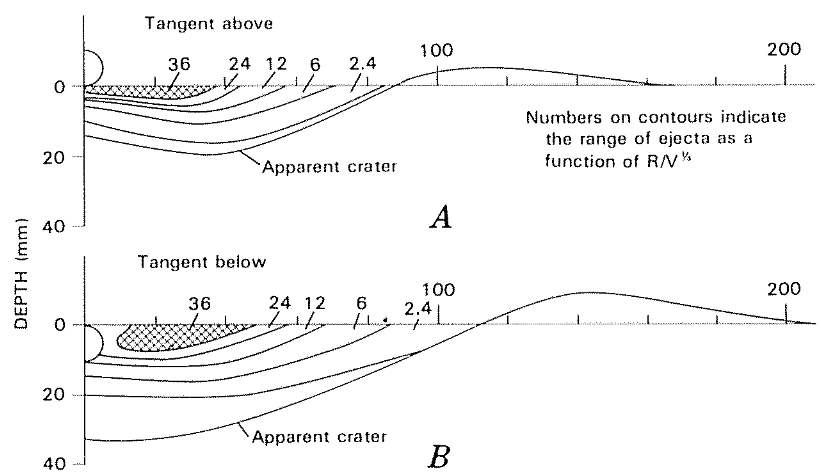

FIGURE 3.18.—Relation between sources of ejecta and range at which it is deposited (from Cooper, 1977, fig. 8). *R*, range; *V*, volume of ejecta; charge, 1.7 g of lead azide; target, dry sand. Results are similar to those of much larger experiments (Cooper, 1977, p. 25). Zones of target material nearest charge were ejected first and to greatest ranges; successively larger and more distal zones were deposited nearer rim.
A. Charge tangential above surface.
B. Charge tangential below surface, similar to energy release of impacts.

from the 25-km-diameter Ries complex crater or ringed basin, southern Germany, which suggests that the inner ejecta was pushed over the rim and moved outward along the surface by gliding and rolling. Ground flow may also have emplaced most ejecta of the 1.7-km-diameter simple crater Lonar, India (Fudali and others, 1980). In contrast, V.R. Oberbeck and his coworkers believe that all ejecta travels in ballistic trajectories and that surface flow is initiated when the ejecta impacts the surface after flight, whereupon it moves outward, together with the abundant excavated local material, under the forces of momentum and gravity. The mechanism proposed by Chao (1974, 1977) would also incorporate local material, because the surface movement occurs under confining pressure, but the proportions of local to primary material might be less than in the ballistic-impact mechanism.

To avoid prejudging the proportions of primary ejecta and local material present, use of the term "continuous deposits" is recommended over "ejecta" for the inner ground-covering material (Oberbeck and others, 1974; Oberbeck, 1975). The term "base surge" is commonly used for the outward flow (for example, Lindsay, 1976) but implies gas- or water-assisted transport, which is unlikely on the Moon. Therefore, the terms "ground surge," "debris surge," or "debris flow" are preferable (Moore and others, 1974; Morrison and Oberbeck, 1975; Oberbeck, 1975).

Deformation and nonballistic ejection

Beyond the sphere of shocked material that is launched into ballistic flight, other target material is less highly shocked but is deformed and sheared. Some of this material is pressed downward and outward along the crater floor and walls in curving paths that resemble those that precede the ballistic ejection (Dence and others, 1977; Croft, 1980). Part of this peripheral material may surge over the walls and exit the crater at very low velocities without leaving the surface.

Additional shock-damaged material is not permanently ejected. Some may be lofted above the crater and fall back inside; other material is mildly brecciated or fractured in place without significant dislocation. Both the fallback and the inplace material form a breccia lens in the bottom of the crater that grades downward and outward into a zone of fractured rock (Shoemaker, 1960, 1962b, 1963; Chao, 1977; Dence and others, 1977, p. 250–253).

The volumes of the cavity from which material was ejected and of the deformed zone may obey different scaling laws (Dence and others, 1977, p. 266–268; Croft, 1980, 1981). In general, a representative linear dimension of a crater—say, the radius or the cube root of the volume—will scale to the kinetic energy of impact (Shoemaker, 1962b; Shoemaker and others, 1962a; Baldwin, 1963; Gault and Moore, 1965; Gault and others, 1968b; Gault, 1970, 1974; Cooper, 1977, p. 16–24; Dence and others, 1977, p. 264–271; Roddy and others, 1977, p. 1133–1296; Melosh, 1980). This linear dimension is also controlled both by gravitational attraction, which inhibits lofting and flight of ejecta, and by rock strength, which influences dissipation of shock energy. Target strength becomes less important, and gravity more important, with increasing impact magnitude; gravity dominates in craters larger than about 100 m in diameter (Moore and others, 1963; Gault and Moore, 1965; Gault, 1974; Chabai, 1977; Gault and Wedekind, 1977; Gaffney, 1978). Smaller craters are created for a given impact kinetic energy when gravity dominates than when strength dominates. In large craters and basins, the excavation cavities may be "gravity craters," whereas their exterior zones may be "strength craters" (Croft, 1980, 1981).

Various terms, most of them used in more than one sense, have been applied to the excavated and nonexcavated parts of a crater. Both "transient crater" and "true crater" have been used to describe the combined zones out to the limit of the nonexcavated breccia, before modification by slumping. However, the term "transient crater" commonly denotes a stage in the cavity growth. "Apparent crater" has been used to denote the depression that is seen excluding the inplace breccia; alternatively, it has been defined as that part of the depression which lies below the precrater ground surface. Therefore, the usage of each term by a given author must be checked. In this volume, I avoid these terms because of their ambiguity and use only "excavation cavity," for the cavity from which material has been removed, either permanently or temporarily before falling back.

Peak and terrace formation

The most conspicuous indicator of internal deformation in craters is the presence of central peaks and wall terraces in complex craters (Gilbert, 1893; Baldwin, 1949, 1963; Dence, 1965, 1968; Quaide and others, 1965; Howard, 1974; Dence and others, 1977; Pike, 1980a, b, c). Diameters of complex craters are generally larger than 16 km in the maria and 21 km in the terrae (fig. 3.3; Pike, 1980a, b). Peaks increase in size and complexity in proportion to crater size up to crater diameters of about 40 or 50 km, but diminish in relative size in larger craters (figs. 3.2*C–E*; Murray, 1980, p. 283). Wall failure first appears as scalloping in small and rudimentary complex craters (fig. 3.2*C*; Head, 1976b; Settle and Head, 1979). Continuous terraces, which probably form by base failure (Grieve and others, 1977; Melosh, 1977), are observed in larger complex craters. Within the transition size range, *d/D* ratios also decrease markedly, and still larger craters have broad shallow floors (figs. 3.2*D*, *E*). Thus, peaks, terraces, and relatively shallow floors all seem to be somehow related. However, these features do not become evident at exactly the same diameter; for example, peaks appear before terraces (Smith and Sanchez, 1973; Head, 1976b; Cintala and others, 1977; Smith and Hartnell, 1978; Wood and Andersson, 1978; Settle and Head, 1979; Pike, 1980a, b, c).

Interpretations of the simple-to-complex transition are commonly reduced to a choice between "push" and "pull" mechanisms: Did the walls of a deep bowl-shaped cavity first collapse centripetally into terraces and push up the central peak, or did the peak originate by some type of rebound of the subcrater material that pulled the walls inward to their collapse? The material trajectories and the ultimate geometry would be similar in both cases. Some form of the "pull" model seems to be supported by appearance of peaks before terraces in the sequence of feature development. The issue largely revolves about the question of the original depth and shape of complex craters: Did they grow to *d/D* ratios that are *proportional* to those of simple craters and then collapse in the "modification stage" (Dence, 1968; Dence and others, 1977; Grieve and others, 1977), or did they grow *nonproportionally* and start out with shallower depths (Croft, 1978, 1980; Settle and Head, 1979; Pike, 1980b)?

A variant of the "pull" model involves a more complex excavation cavity, consisting of a deep inner part surrounded by a shallower shelf. Only the central part grows proportionally. A key feature is subhorizontal inward motion of the subcrater material during crater growth (fig. 3.19). Material beneath the central depression is severely deformed and sharply uplifted to become the central peak (Roddy, 1968, 1976, 1977, 1979; Milton and Roddy, 1972; Milton and others, 1972; Wilshire and others, 1972a; Offield and Pohn, 1979). In contrast, strata beneath the shallow floor surrounding the peaks are mildly deformed and are neither uplifted nor downdropped substantially. Support is withdrawn from the walls, which collapse most completely in large craters, where the inward motion is greatest.

Causes of the deformation and of the simple-to-complex transition remain particularly debatable (Quaide and others, 1965; Pike, 1980a, b). Some phenomenon may relate shallow depths of burst, peak formation, and shallow floors. Shallow bursts, which may form peaks in very small craters, have been documented by stratigraphic relations and the orientation of shatter cones in such terrestrial craters as Gosses Bluff, Australia (Milton and others, 1972) and Flynn Creek, Tenn. (Roddy, 1977). Low-density projectiles would release their kinetic energy near the surface because of their shallow penetration (Roddy, 1968, 1977), as would very large projectiles of any density (fig. 3.20). Large bodies penetrate to shallower depths relative to their kinetic energy than do smaller objects, and require more time to be consumed (Baldwin, 1963, p. 164–184). Thus, (1) peaks may form because of the shallow energy release; (2) more energy is directed laterally than in deeper bursts, so that craters are shallow; and (3) energy coupling is sustained over longer times, so that more of the target material is heated than in rapid energy releases (see next section below). Many properties of complex craters and ringed basins (see chap. 4) are explainable in this way.

Shallow bursts do not explain all phenomena, however, because the diameters in the simple-to-complex transition and the morphologic properties of peaks and floors differ from region to region and from planet to planet (Cintala and others, 1977; Pike, 1980a, b). Two factors are commonly proposed as modulators or even as initiators of the complex-cratering process and also of basin-ring formation: (1) differing gravitational attraction at the planets' surfaces

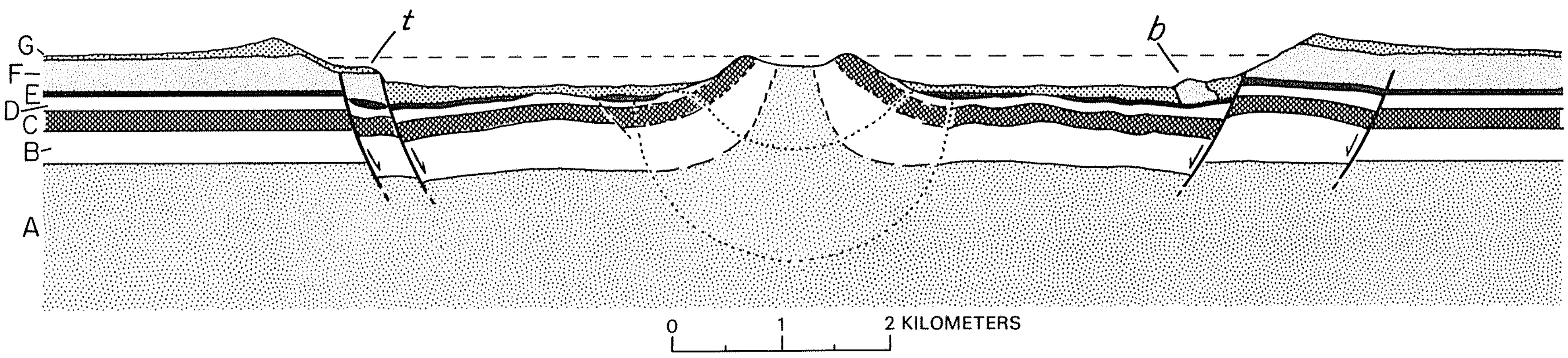

FIGURE 3.19.—Model of formation of features of complex crater, according to Pike (1980b, fig. 9). Only strata A, B, and C are exposed in central uplift, where they dip vertically or steeply. Stratum F has been stripped from crater, although it forms a slump block (b). Stratum G is composed of ejecta and intracrater breccia. Faults creating terraces (t) pinch out at shallow depths. Arcuate dotted lines indicate zones of deformation in center. Modeled after four complex craters on Earth; scale applies to average horizontal and vertical dimensions of those craters.

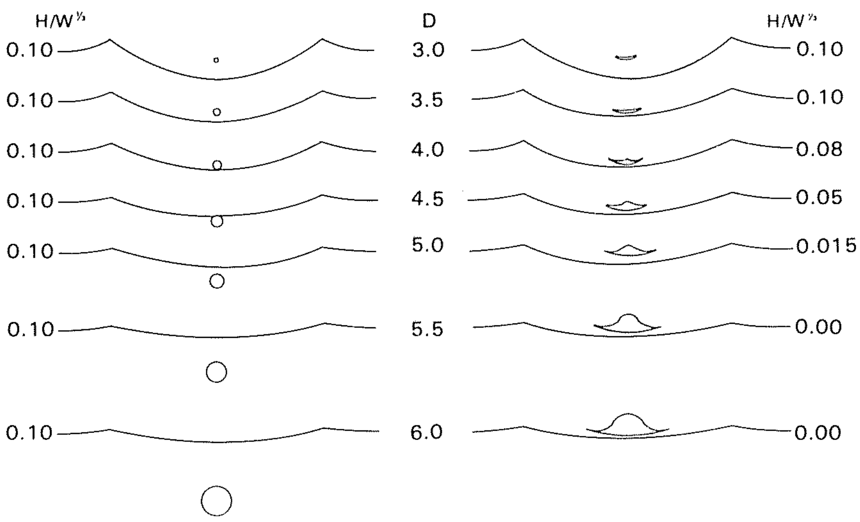

FIGURE 3.20.—Relative depth of penetration and effect on crater diameter of large and small projectiles (Baldwin, 1963, fig. 29). *D*, logarithm of diameter (in feet). Depth/diameter ratios are typical of lunar craters. $H/W^{1/3}$, scaled depth of burst; H, depth (in feet); W, explosive energy (in pounds of TNT equivalent). Left panel, penetration assumed beneath original ground surface to two projectile diameters for all seven sizes of craters; impact velocity is set at 10 mi/s; unlikely result of very shallow crater overlying deep burst is obtained for largest craters. Right panel, more realistic variable and shallow depths of penetration, including surface bursts for two largest sizes. Projectiles flatten during consumption by shock wave (Baldwin, 1963, p. 167).

(Hartmann, 1972a; Gault and others, 1975; Pike, 1980a, b), and (2) substrate properties, especially layering. Discontinuities between layers affect the coupling of impact energy into the target and refract and reflect the shock waves (Sabaneyev, 1962; Oberbeck and Quaide, 1967, 1968; Quaide and Oberbeck, 1968; Rinehart, 1975; Head, 1976b; Oberbeck, 1975, 1977; Piekutowski, 1977; Hodges and Wilhelms, 1978). Different stratification may explain the different simple-to-complex transition diameters between maria and terrae. Gravity or substrate properties, however, cannot be the sole factor in complex-crater formation, considering that peaks appear in all sufficiently large craters on all impacted moons and planets (Pike, 1980a, b).

In summary, shallow energy releases, strong gravitational attraction, and sharp contrasts in target stratification all seem to enhance formation of the peaks, shallow floors, and terraces characteristic of complex craters. Different combinations of these factors among planets or on a single planet, such as the Moon, yield quantitatively different results. None of these factors, however, may be the fundamental cause of complex craters. Changes in the basic physical effects of impact above some energy threshold (for example, Melosh, 1980) ultimately may be found to be more significant.

Impact melting

Estimates of the amount and stratigraphic relations of impact melt are important to the interpretations of lunar breccia presented later in this volume (chaps. 9, 10). Projectile size, impact velocity, and density of both the projectile and the target affect the partitioning of energy among mechanical excavation, deformation, and impact melting (Baldwin, 1963; Gault and Heitowit, 1963; Gault and others, 1968b, 1975; Dence, 1971; Ahrens and O'Keefe, 1972; O'Keefe and Ahrens, 1977; Kieffer and Simonds, 1980; Melosh, 1980). High-velocity impacts of small projectiles generate small amounts of very hot melt, whereas slow large impacts generate larger amounts of less thoroughly melted material (Rehfuss, 1974; O'Keefe and Ahrens, 1975, 1977, 1978; Grieve and others, 1977, p. 809; Lange and Ahrens, 1979). For the same mass and velocity—that is, the same kinetic energy—low-density projectiles generate more melt than do dense projectiles (Kieffer and Simonds, 1980). The melt traps much of the heat energy of the impact and does not contribute to the excavation process except for the melt that may have been lost by early jetting (Shoemaker, 1962b, p. 316; Gault, 1974). Therefore, in proportion to kinetic energy, large impactors melt more material and eject less fragmental material than do small impactors.

Emplacement of impact melt is one of the last processes to run its course during a cratering event but one of the first to be initiated. Melt originates in the impact zone and is pressed outward along the walls of the growing cavity (fig. 3.21). On the Moon, what appear to be flows of impact melt are superposed on crater walls and flanks, and pools of melt rest in depressions both inside and outside the rim crest (figs. 3.22, 3.23). These relations indicate that the melt is still mobile after the fragmental ejecta leaves the crater (Shoemaker and others, 1968; Guest, 1973; Moore and others, 1974; Howard, 1975; Howard and Wilshire, 1975; Schultz, 1976b, p. 228–237; Hawke and Head, 1977a). Apparently the melt sloshes over the rim along with some of the last fragmental ejecta, and locally flows back downward into the cavity after terracing ceases (Howard, 1975; Howard and Wilshire, 1975; Grieve and others, 1977; Phinney and Simonds, 1977).

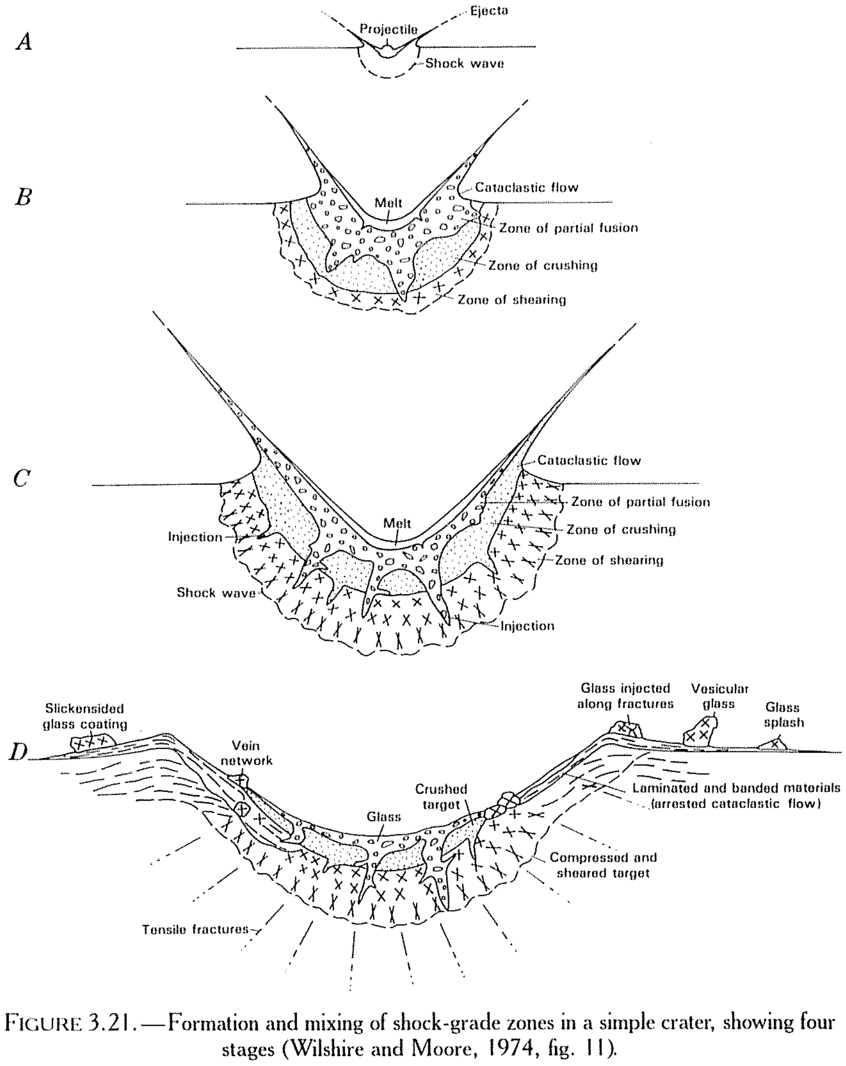

FIGURE 3.21.—Formation and mixing of shock-grade zones in a simple crater, showing four stages (Wilshire and Moore, 1974, fig. 11).

Formation times

Impact craters form in less than a minute (Melosh, 1980, p. 80). Schmidt (1981) suggested that formational time is proportional to the sixth power of the excavated volume.

In some terrestrial craters, the melt contains breccia from the peak (Simonds and others, 1976b). This observation confirms that peaks form early in the cratering sequence, as suggested above, because impact melt solidifies very quickly. In large craters on the Canadian shield, the time between impact and melt solidification was about 100 s (Onorato and others, 1976, 1978). Final cooling below temperatures able to metamorphose the melt and clasts required less than 2,000 years (Onorato and others, 1978).

IMPACT BRECCIA

Terrestrial analogs

Studies of impact-generated terrestrial materials, which began during the 1960's in conscious preparation for the Apollo landings (Chao, 1967; Engelhardt, 1967, 1971; French and Short, 1968; French, 1977, p. 155), have provided essential clues for interpretations of the returned samples. Progressive mineralogic and textural changes in the target rock have been correlated with intensity of the outward-decaying shock wave (French and Short, 1968; Dence and others, 1977; Robertson and Grieve, 1977).

Among the first impact-generated materials to attract attention were *tektites*, small, glassy, aerodynamically shaped objects found in strewn fields at several terrestrial localities. They have been thought to be lunar in origin (O'Keefe and Cameron, 1962; O'Keefe, 1963) but are much closer in composition to the target materials of terrestrial craters (King, 1976, chap. 2; Glass, 1982, chap. 6). The tektites of each strewn field probably originated during early jetting of very hot material from a terrestrial impact (fig. 3.21*A*; Kieffer and Simonds, 1980), were carried to various altitudes in and above the atmosphere by a fireball, and were dispersed by gases in the fireball and by stratospheric winds (Jones and Sandford, 1977).

Lunar studies have depended heavily on analogies to the Ries crater in Germany and the numerous craters or ringed basins on the Canadian shield. The diameters of the most conspicuous rings of the three largest Canadian craters, Manicouagan and West and East Clearwater, are 65, 32, and 23 km, respectively; however, the exterior ejecta has been eroded away and the excavation diameters are uncertain. The Canadian craters have furnished much data about shock metamorphism and impact melting (Dence, 1968, 1971; Grieve and others, 1974, 1977; Grieve, 1975, 1978, 1980; Floran and Dence, 1976; Simonds and others, 1976a, b, 1978a, b; Dence and others, 1977; Phinney and Simonds, 1977; Phinney and others, 1977, 1978; Robertson and Grieve, 1977; Floran and others, 1978; Grieve and Floran, 1978). The larger craters possess massive interior sheets of impact-melt rock, about 100 m thick, which texturally resembles igneous rock. The 25-km-diameter Ries crater has furnished fewer impact-melt rocks (as parts of the deposit called suevite) but abundant unshocked fragmental ejecta (mostly in the Bunte Breccia) (Engelhardt, 1967; Dennis, 1971; Chao, 1974, 1977; Gall and others, 1975; Chao and Minkin, 1977; Pohl and others, 1977; Hörz and Banholzer, 1980). Representative types of terrestrial impact materials from these and other craters have been illustrated and compared with lunar impact materials by Stöffler and others (1979).

Lunar-terra samples

Except for tektites, the whole range of shock grades is much better represented on the lunar terrae than on the eroded Earth. Terra-breccia deposits display complex shock effects, ranging from cataclasis of monolithologic rocks, through solid-state metamorphism, to intricate assemblages of cogenetic and foreign clasts within clastic and impact-melted matrices (see fig. 2.7, chaps. 8-10, and summaries by James, 1977; Phinney and others, 1977; Stöffler and others, 1979, 1980; Taylor, 1982, p. 187–201). Some individual specimens consist entirely of breccia or entirely of melt rock (fig. 2.8), and have been so designated in the literature. However, these rock types must have been parts of deposits containing both melted and unmelted materials, and so the term "breccia" is used here as a general term for lunar impact materials.[3.1]

[3.1]Only the breccia that forms deposits of the terra bedrock is discussed here. At the time of the first two Apollo landings, the only known breccia was that created in regoliths, because the terrae had not yet been visited. The regolith breccia (also called soil breccia, microbreccia, glassy breccia, vitric-matrix breccia, and numerous other names) constituted an obviously different type of material from the igneous basaltic lavas found at those sites. When the much coarser, more massive, more complex, and more extensive bedrock breccia became known, the nomenclature did not fully adapt to the differences. Some petrologic literature does not clearly distinguish between regolith breccia, formed by innumerable small impacts near the lunar surface, and bedrock breccia, formed by fewer and larger impacts (also called "megaregolith"). In this volume, "breccia" denotes bedrock breccia unless otherwise indicated, and "megaregolith" is not used because it obscures the fact that the bedrock breccia forms discrete strata.

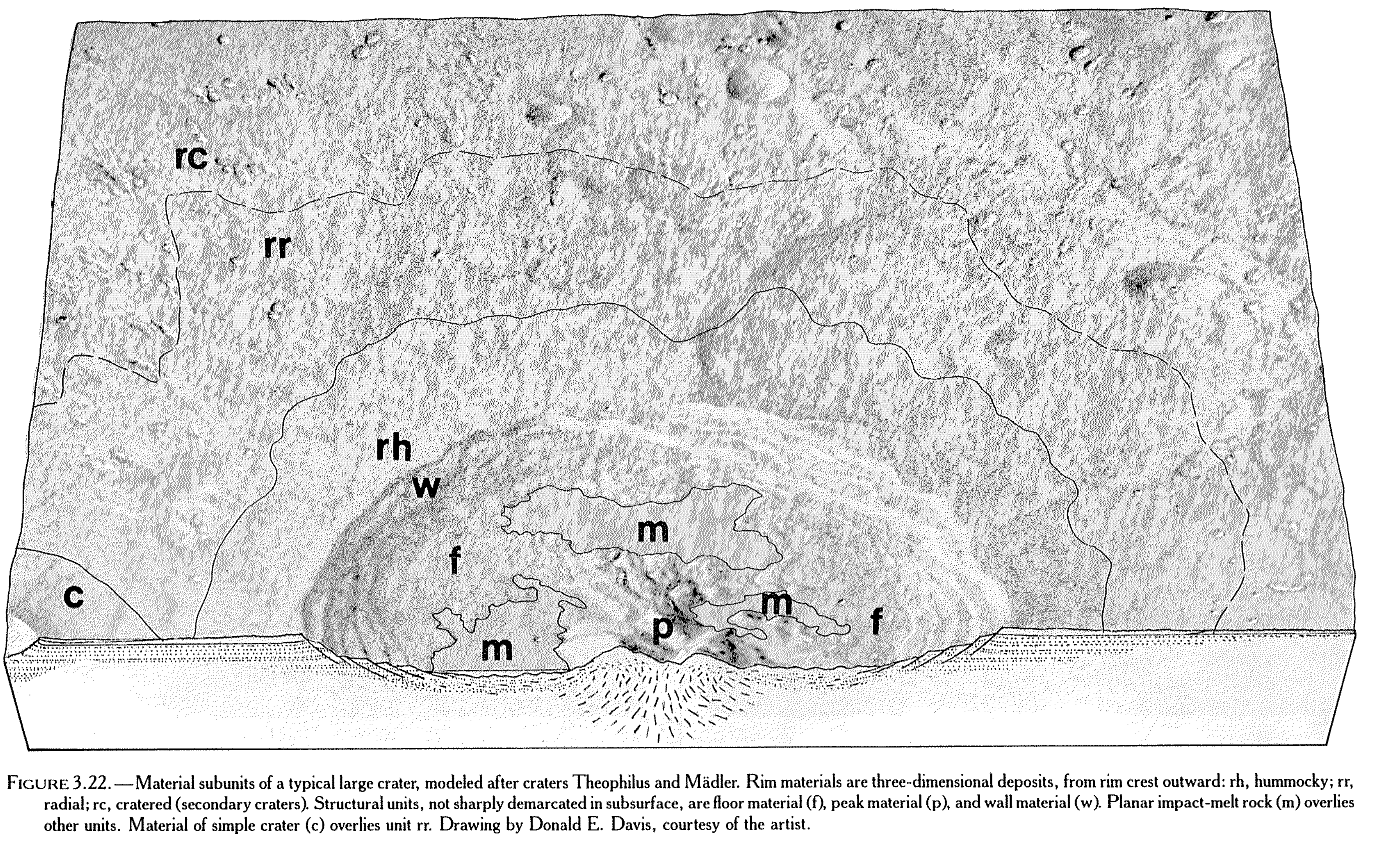

FIGURE 3.22.—Material subunits of a typical large crater, modeled after craters Theophilus and Mädler. Rim materials are three-dimensional deposits, from rim crest outward: rh, hummocky; rr, radial; rc, cratered (secondary craters). Structural units, not sharply demarcated in subsurface, are floor material (f), peak material (p), and wall material (w). Planar impact-melt rock (m) overlies other units. Material of simple crater (c) overlies unit rr. Drawing by Donald E. Davis, courtesy of the artist.

Some features of breccia deposits can be related to the outward decrease in shock intensity during the growth of a crater (fig. 3.21), whereas others illustrate the textural and compositional complexities that impact cratering induces.

Impact melts that have glassy or crystalline textures most like those of igneous basalt presumably were formed near the impact zone (for example, *ophitic* texture, in which pyroxene encloses less abundant plagioclase laths, or *subophitic* texture, in which pyroxene partly encloses a subequal volume of plagioclase laths; compare figs. 2.6, 2.8). *Poikilitic* texture in which numerous small, more nearly equant plagioclase grains and other debris are enclosed by large pyroxene crystals is considered to be a sign that many minute clasts were incorporated in the impact melt (Nabelek and others, 1978). Melt rocks with these various textures were recovered from most sampling sites, most abundantly from the Apollo 17 terra stations (see chap. 9). Melt-poor friable fragmental breccia, likely formed in the outer parts of excavation cavities, was returned from all the terra landing sites, most abundantly by Apollos 14 and 16 (see chaps. 9, 10). Some material derived from the outer parts of the excavation cavities and ejected late in the cratering sequence consists of coherent blocks (fig. 3.21*D*).

This zoning is muddied by the turbulent processes that characterize energetic impacts. Melted material of projectile and target that is not jetted is pressed into the growing cavity (fig. 3.21*B*). As the crater grows, this material, formed near the energy-release zone, is injected into the less highly shocked but fragmented rock in outer zones (figs. 3.21*B–D*; Dence, 1971; Wilshire and Moore, 1974; Simonds and others, 1976a, b, 1978b; Chao and Minkin, 1977; Grieve and others, 1977; James, 1977; Grieve and Floran, 1978; Stöffler and others, 1979). Thus, melt rock appears as matrices and dikes among less highly shocked fragments (fig. 3.21*D*). Unmelted but crushed clastic debris may be similarly injected. These processes are illustrated by *dimict breccia,* consisting of fragmental breccia and melt rock showing mutual intrusion and inclusion relations (James, 1977, p. 647; 1981; Stöffler and others, 1981).

Such mingling of shock grades can be quite thorough: Rock and mineral fragments, shocked to varying degrees, may be engulfed by impact melt (fig. 2.7). Moreover, various breccia and melt types are interbedded in the crater interiors (Stöffler and others, 1979). This bedding varies in sequence and lithology for craters of different sizes and different target materials (Stöffler and others, 1979; Stöffler, 1981), and commonly juxtaposes materials that have experienced a wide range of shock pressures. At any stage in the cratering process, the material being ejected may consist of a mixture of complete melt, fragment-laden melt, and unmelted fragments.

Shearing of material from the crater walls and transporting it outside the crater further mixes the ejecta and streaks it into bands or pods. Glass-coated striated fragments evincing shearing during ejection or transport are known (Wilshire and Moore, 1974). Some samples even appear to be accretionary bombs (Stoeser and others, 1974; Wood, 1975d; Spudis and Ryder, 1981). Mixing with the substrate material increases outward from the crater because of surface transport and increasing secondary-impact velocity of the ejecta. Lunar breccia containing clasts of melt formed in the same impact that emplaced the breccia has been referred to as "suevite"; clasts of impact-melted rock in fragmental deposits analogous to the Ries Bunte Breccia predate the deposit (Stöffler and others, 1979, 1980). However, distinguishing the two types of deposit is difficult on the Moon, where the source crater of a breccia is commonly unknown.

After the deposits come to rest, the intimate mixture of hot or superheated melt and warm or cold fragments of varying compositions in all conceivable combinations of grain size and abundance leads to further modifications of the deposit (Simonds, 1975; Simonds and others, 1976a, b). Melt and hot clasts are differentially quenched during the rapid initial cooling of the deposit. Sharp local differences in crystallinity, interface texture, and remaining content of fragments may arise. The second, much slower stage of cooling further metamorphoses the deposit and underlying materials. The terrestrial metamorphic terms "granoblastic" or "granulitic" (anhedral grains of subequal size) are applied to many lunar textures believed to have arisen from thermal metamorphism (Warner and others, 1977; Taylor, 1982, p. 198–200). Thus, the complexities arising in a single impact may be so great that they mimic the relations arising from multiple events (Simonds, 1975).

The complexities of lunar impact deposits at the scale of the outcrop or the hand specimen are not surprising in view of the complexity of each individual impact and the fact that each volume of material may be similarly reworked by many subsequent impacts. Consequently, any attempt to categorize lunar impact materials is bound to fall short of reality. The most useful in a series of attempts

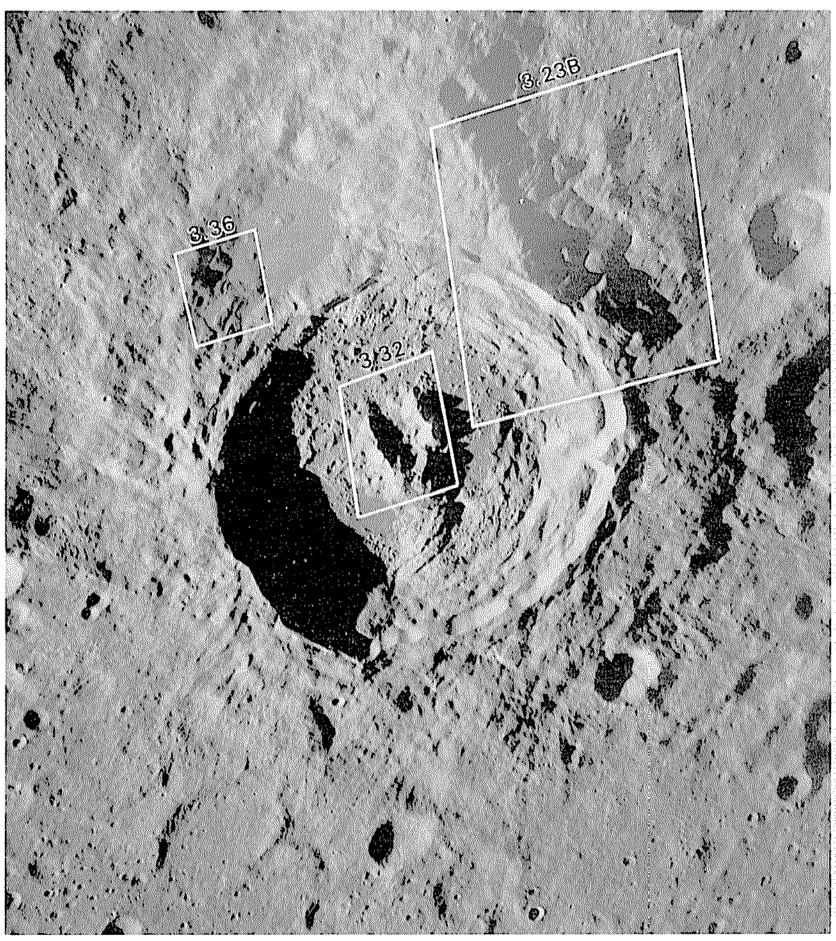

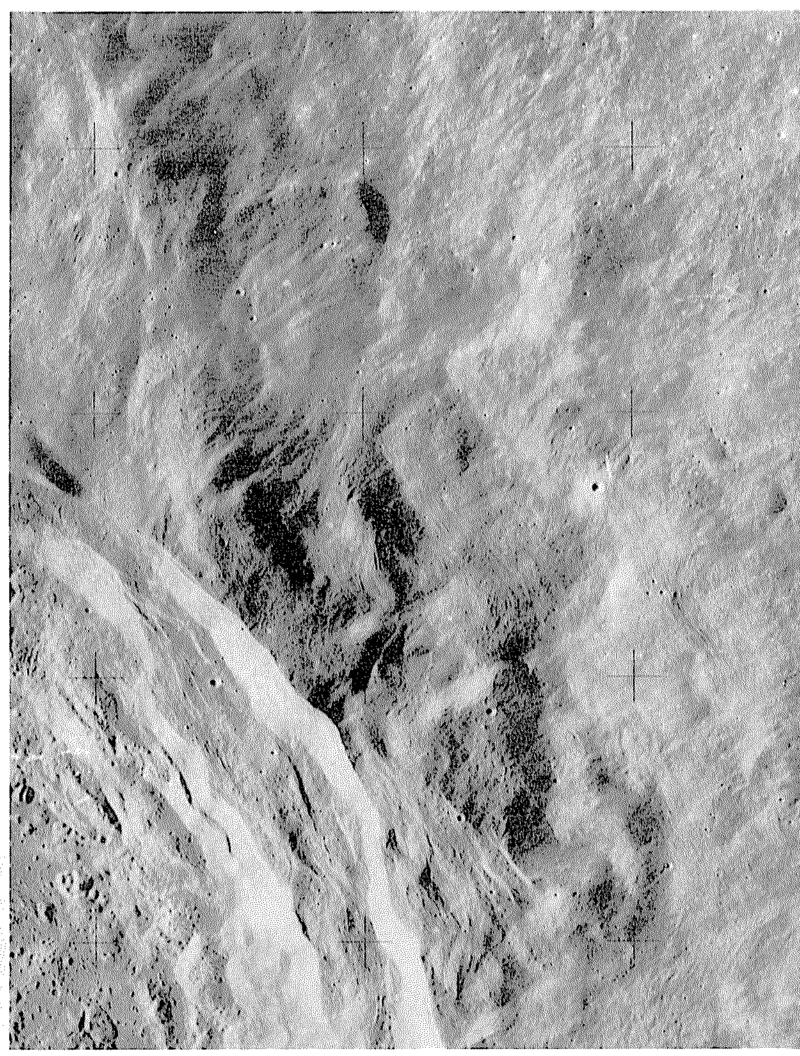

FIGURE 3.23.—Very fresh crater King on farside (77 km, 5° N., 121° E.).

A. Entire crater. "Lobster claw" central peak connects with wall and is overlain by lower wall material (enlarged in fig. 3.32). Pool of impact melt outside northwest rim is enlarged in figure 3.36. Apollo 16 frame H–19580.

B. Northeast rim, showing concentric textures of rim material downdropped along with terraces inside rim and locally lying outside rim (lower part of photograph). Gradation from concentric to radial pattern of outer rim material indicates increasing radial-flow component of outer material. Apollo 16 frame M–1579.

was probably that by Stöffler and others (1980), who compiled a long list of earlier names that should greatly aid the reader of the technical literature. Stöffler and others (1980) used textures and structures, which are signs of the process that formed the rocks, as their main basis for classification. Essentially, this classification describes matrices as either fragmental, crystallized from a melt, still glassy or partially devitrified, or metamorphosed. Clast content can be described according to need. From the geologic point of view, this classification improves upon those based on chemical composition. Many purposes are served by a still simpler breakdown into clast-rich and melt-rich (clast-poor) breccia types.

Reconstruction of the history of lunar breccia deposits severely challenges the petrologist, geochemist, and geologist. The place and process of original formation of the clasts and of the raw materials for the melts (chap. 8) must be disentangled from the process by which they arrived at the place where they were collected (chaps. 9, 10). Each clast may yield a different isotopic age, attesting to many endogenic and impact events in the sample's history, or only to incomplete migration of Ar, Rb, and Sr isotopes (chaps. 9, 10). The crater or basin in which most of them originated can only be inferred. Unsuspected complexities in the process of forming craters and, especially, basins may have shaped the materials of the lunar terrae.

SUMMARY OF CRATER-MATERIAL ORIGIN

Introduction

Around almost all impact craters, the processes described above have created similar patterns of continuous ejecta grading outward to secondary craters. The major apparent differences among craters are between the interiors of simple and complex craters. Partly understood variations in the target material, such as in structure, cohesion, and topographic relief, also affect the details of morphology; and variations in projectile velocity, density, and impact angle affect both the morphology and the proportions of melted and ejected material. Nevertheless, the basic morphologic patterns of impact craters are much more alike than those of volcanic craters.

This similarity has greatly aided the reconstruction of lunar geologic history. Stratigraphically based lunar geologic mapping has become increasingly effective as the analogies between modified and unmodified deposits have become clearer. The material subunits in and around craters were generally recognized as stratigraphic entities when they were mapped geologically in the 1960's (Mutch, 1970, p. 165–175; Wilhelms, 1970b, p. 40–42), and their mapped limits remain generally valid. The interpretations of some units, however, have changed (compare Schmitt and others, 1967, and Howard, 1975). To enable modern use of these maps, this section updates the interpretations of each class of unit on the basis of the newer research summarized above, and suggests what rock types are likely to occur in each unit and in the analogous units of basins.

Rim material

A raised rim, formed by uplift of the target and by deposition of ejecta, surrounds the crater. The geologic unit "rim material" (a member of the formation "crater material") essentially corresponds to the continuous ejecta (fig. 3.22). Smooth, clean-looking rim surfaces may have been stripped of ejecta by late-stage radial flow (Guest, 1973). On the near flanks of simple craters, ejecta materials have been deposited in inverse order of their original sequence. Original stratigraphic units are more jumbled in complex craters (Hörz, 1981). Impact melt forms ponds in depressions and coats other parts of the rim (figs. 3.23). The deposits also probably incorporate clasts and veins of impact-melt rock along with fragmental ejecta. The relative amounts of melted and unmelted ejecta depend on factors of projectile size, density, and velocity, and on such target properties as density and volatile content.

The hummocky facies of rim material (a submember) consists of late-emplaced material that was derived from near the crater wall and overlies the structurally uplifted and outthrust zone of larger craters. Blocks of relatively undeformed material are scattered on the rim (figs. 3.2*A*, 3.23*B*). The rim's generally concentric structure attests to final emplacement by outthrusting (fig. 3.23). In places, younger crater rims have breached older rims, and the hummocky materials flowed rapidly (fig. 3.24) or sluggishly (fig. 3.25) into the gap. Therefore, the deposits were emplaced along the surface. Around old craters, the hummocky rim facies, without the topographic subtleties of young craters, is the only distinguishable rim material (fig. 3.26).

Outward from the hummocky rim material, ridges in radial and herringbone patterns form a continuous-appearing wreath with irregular lobate margins (fig. 3.22). In the well-photographed complex craters illustrated here, the radial rim facies (submember) is clearly an outward gradation of the hummocky rim material (figs. 3.23, 3.24, 3.27). Surface flow after ejection is indicated by the textures curving from concentric to radial patterns (figs. 3.23*B*, 3.24, 3.27*A*). Some of the ejecta apparently was molten (fig. 3.27*B*). The gradation with materials at the rim crest and the content of impact melt indicate that the ejected ground-flow materials are dominated by primary ejecta. The outer part of the radial rim material, however, contains locally derived material because substrate material was incorporated either by ground flow of the ejecta under confining pressure or during ballistic emplacement of the ejecta.

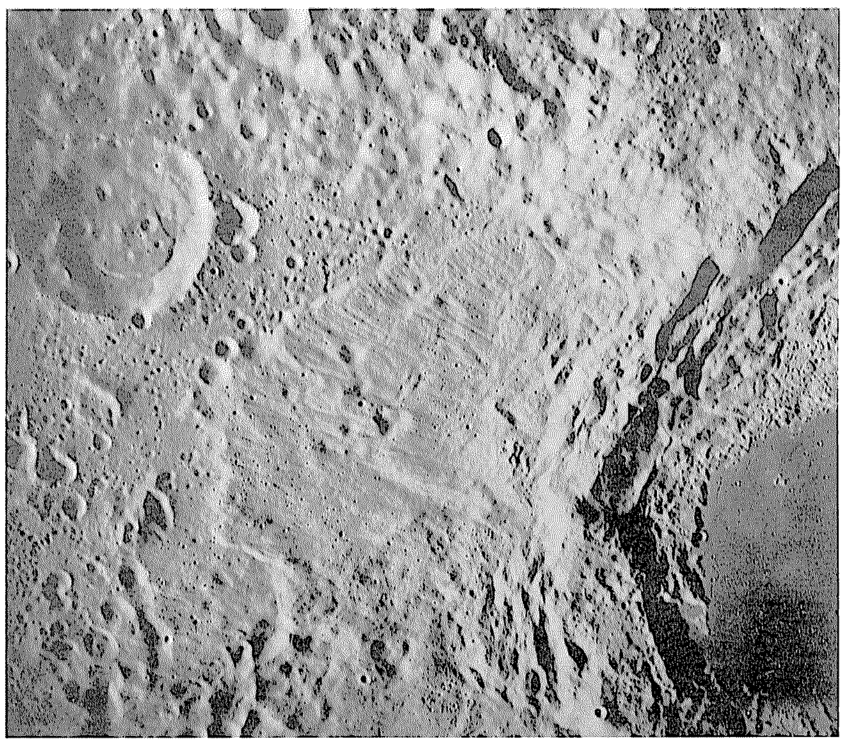

FIGURE 3.24.—Lineations of northwestern ejecta of crater Tsiolkovskiy, indicating ground surge beyond concentric near-rim deposits. Smaller crater in upper left, probably filled with additional Tsiolkovskiy ejecta, is Lütke (39 km). Apollo 17 frame M–2608.

FIGURE 3.25.—Concentric ejecta of crater Shirakatsi (51 km, left), pushed through gap in rim of older or nearly contemporaneous crater Dobrovol'skiy (38 km). North of Tsiolkovskiy, centered at 13° S., 129° E. Apollo 17 frame M–2608.

At some radius, ballistically generated secondary craters appear. Much of the ejecta thrown from secondaries has a herringbone pattern that originated by intersection of cones of their ejecta (figs. 3.4*C–F*, 3.6, 3.7). In the ideal case, derivation of the farthest-thrown materials from near the impact zone (fig. 3.18) means that the secondaries were formed by highly shocked material from shallow depths in the primary target. Thus, whatever primary material is recovered from the secondary ejecta will contain impact melt or other high shock grades, whereas the local material in the secondary ejecta should be less shocked because of the lower kinetic energies of the secondary impacts. The proportions are not known, but locally derived material probably increases with distance from the primary crater. Some geologic maps distinguish a rim-material facies called cratered rim material (fig. 3.22) and identify the underlying unit of which it is composed (Ulrich, 1969).

The ejecta of young secondary craters commonly appears as rays or bright splashes of freshly exposed material (figs. 3.4*A*, *C*, 3.6, 3.28). Most of this ray material was probably excavated from the local terrain by secondary impacts. Many investigators of rays have suspected that fine primary ejecta also composes parts of rays (for example, Baldwin, 1963, p. 358; Schultz, 1976a, p. 204; Pieters and others, 1982). Absolute dating of Copernicus and Aristillus depends on the interpretation that the samples recovered on rays hundreds of kilometers from those craters contain primary ejecta (see chap. 13).

Wall material

Wall material is a mixed unit that includes materials of the terraces and all the slumps, debris, and impact melt that coat crater walls. Walls may expose precrater strata (fig. 3.29). Edges of the terraces may also contain precrater target rock, and tops may expose downdropped rim material. Depressions in the terrace tops, which are most common on the rears of the outward-tilted downdropped surfaces, commonly contain pools of flat-surfaced material now recognized as impact melt (figs. 3.2*D*, 3.23*B*; Howard, 1975; Howard and Wilshire, 1975; Hawke and Head, 1977a). Dribbles or cascades of additional melt or debris, commonly bounded by levees resulting from the flow, connect some terraces and the floor (fig. 3.30; Howard, 1975). These melt features, which are seen only on high-resolution photographs, merely contribute to the overall rough appearance of the walls as seen on telescopic photographs. Coarse wall hummocks are probably slumps (fig. 3.27*A*).

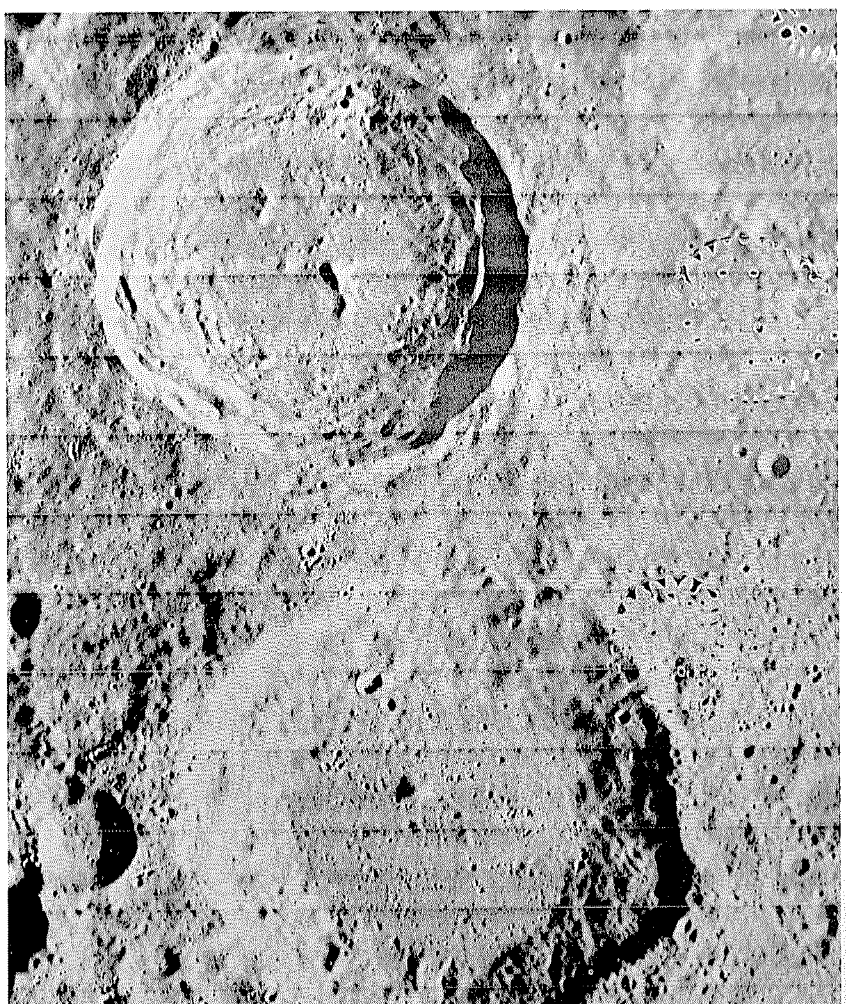

FIGURE 3.26.—Ejecta of moderately fresh (Eratosthenian) crater Werner (70 km, 28° S., 3° E., above), superposed on crater Aliacensis (80 km, below), whose subdued walls, raised rim wreath, and central peak were probably similar to those of Werner when first formed; Aliacensis-radial ejecta is no longer visible. Rim nearest Werner is more highly degraded than distal rim. Orbiter 4 frame H–100.

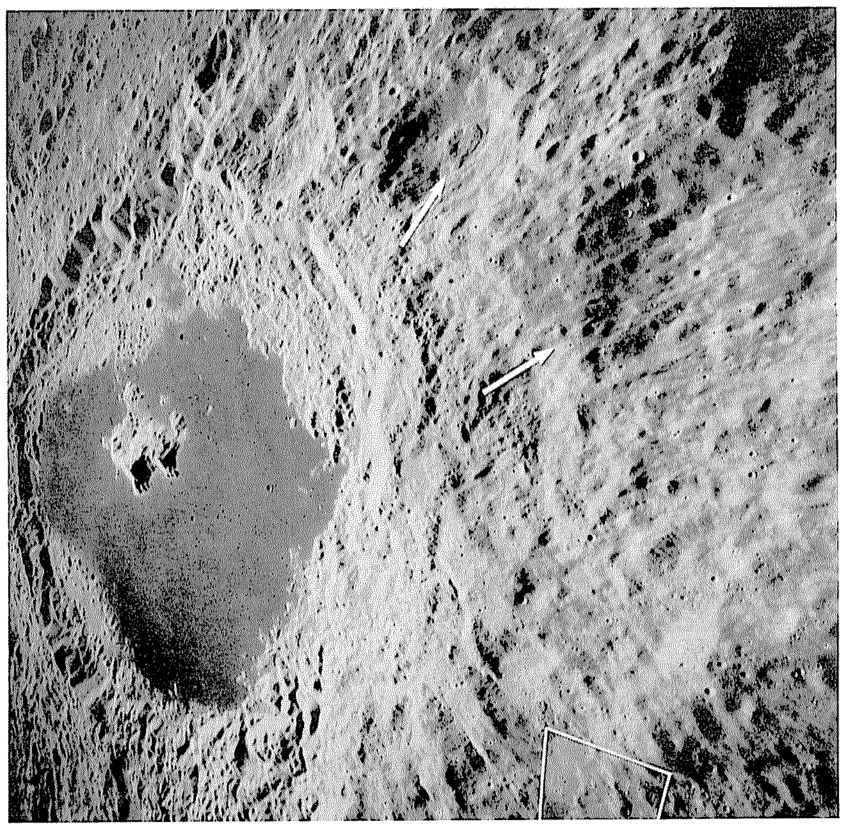

A

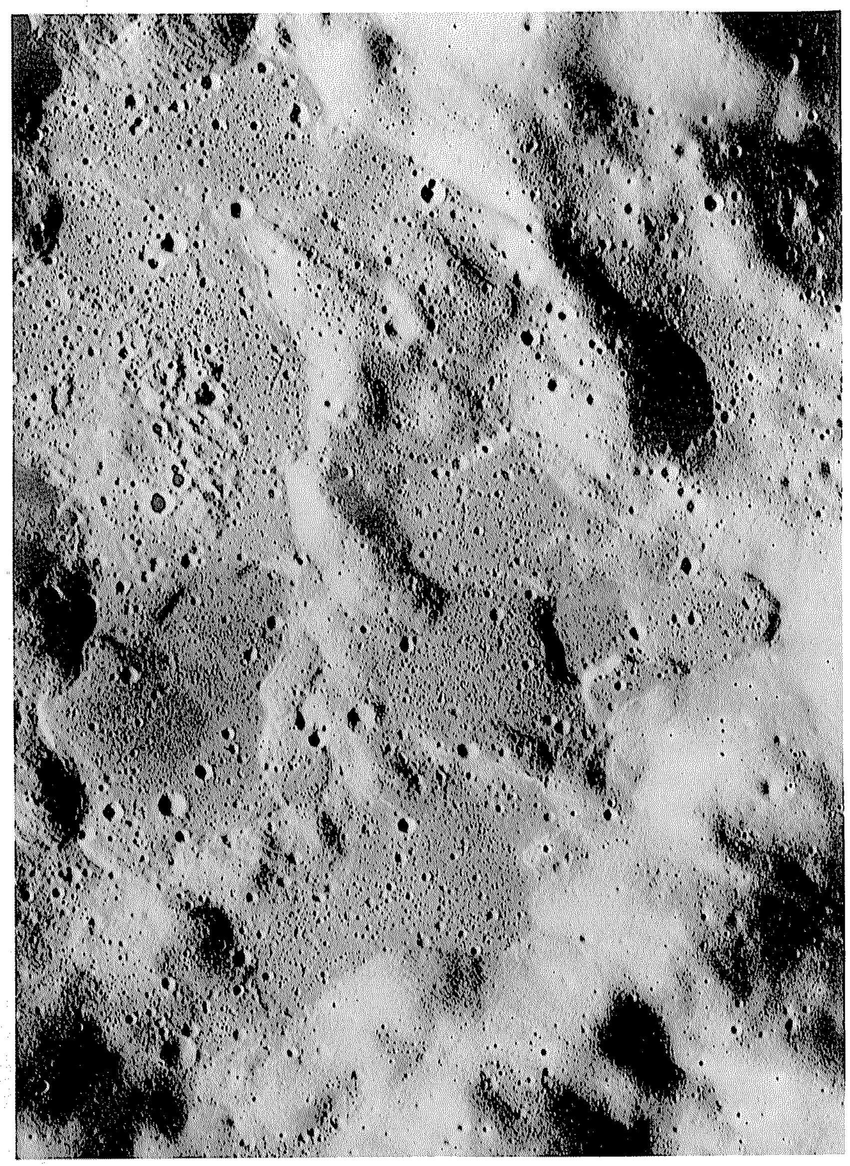

B

FIGURE 3.27.—Eastern ejecta of Tsiolkovskiy (180 km).

A. Ground-surge emplacement is indicated by diversion from concentric to radial lineations (arrows). Impact melt is visible at upper arrow and in box at bottom. Apollo 15 frame M–757.

B. Impact melt, partly enclosed in box in figure 3.27*A*, covers radial ejecta. Apollo 15 frame P–9580.

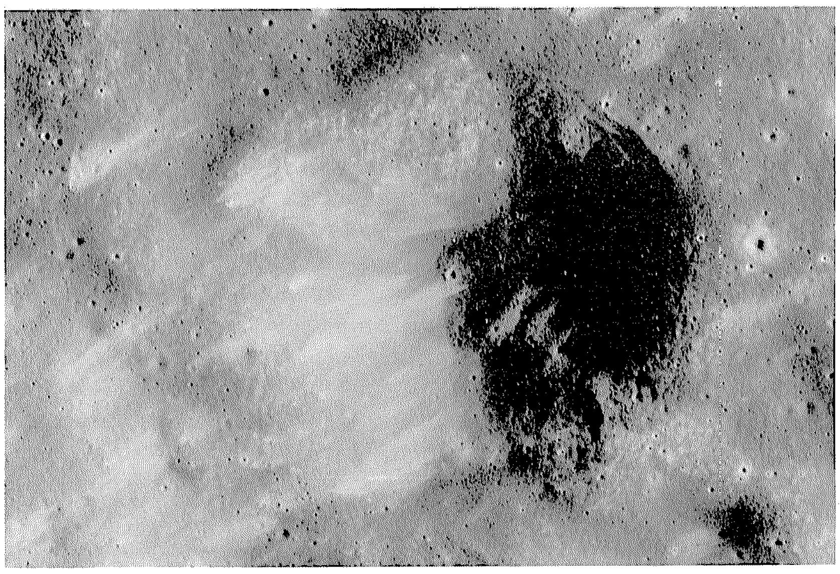

FIGURE 3.28.—Splashes of bright material dug from beneath darker surficial layers by secondary-impact craters of a crater out of scene to lower left. Crater in picture is about 5.5 km across; near west rim of Gagarin. Apollo 15 frame P–8941.

On many geologic maps, material slowly uncovered or displaced downslope on crater walls is mapped as a unit called bright slope material (Mutch, 1970, p. 166–169; Wilhelms, 1970b, p. 39). This unit was early recognized by geologic mappers and ascribed to renewal of exposure of lunar rock by downslope movement (Shoemaker and Hackman, 1962, p. 297; Shoemaker, 1965, p. 128); it was generally assigned a Copernican age regardless of the age of the underlying unit. A substantial content of fresh material has been confirmed by spectral studies (see chap. 5), and all high-resolution photographs of steep lunar slopes reveal mass-wasted debris deposits (figs. 3.31–3.33). The time of exposure of materials in the colluvium at the bases of massifs at the Apollo 15 and 17 landing sites has been dated isotopically at tens or hundreds of millions of years, in contrast to several aeons for the source rock. The colluvium and slope debris contain material foreign to the source and introduced by impacts. The oldest (darkest) slopes probably have accumulated the most exotic material (fig. 3.31).

Peak material

The geologic unit "peak material" was probably derived from greater depths than any other lunar-crater material because the material in peaks formerly lay beneath the excavated part of the crater (fig. 3.19). Peaks range considerably in morphology from low hills and single centralized pinnacles, through multiple jagged peaks clustered around a center, to dispersed smaller arrays (figs. 3.2*C–E*, 3.29, 3.32–3.35, 4.2). All these forms are consistent with uplift mechanisms. Peaks probably formed during crater excavation by intensive

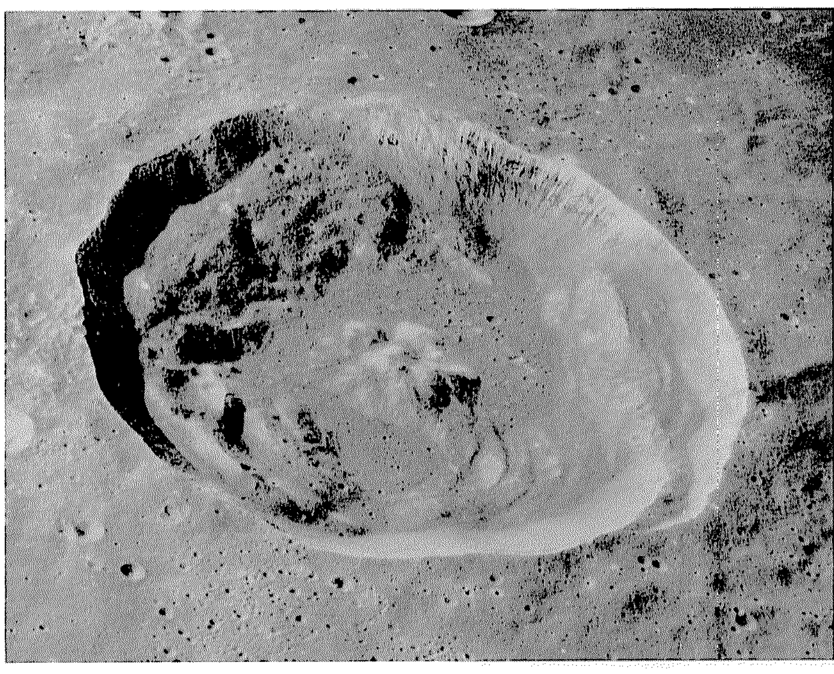

FIGURE 3.29.—Crater Euler (28 km, 23° N., 29° W.), showing wall materials weakly coalesced into terraces at bottom and uncoalesced in upper left. Precrater stratigraphic units are evident by albedo differences on upper right wall. Apollo 15 frame P–10274.

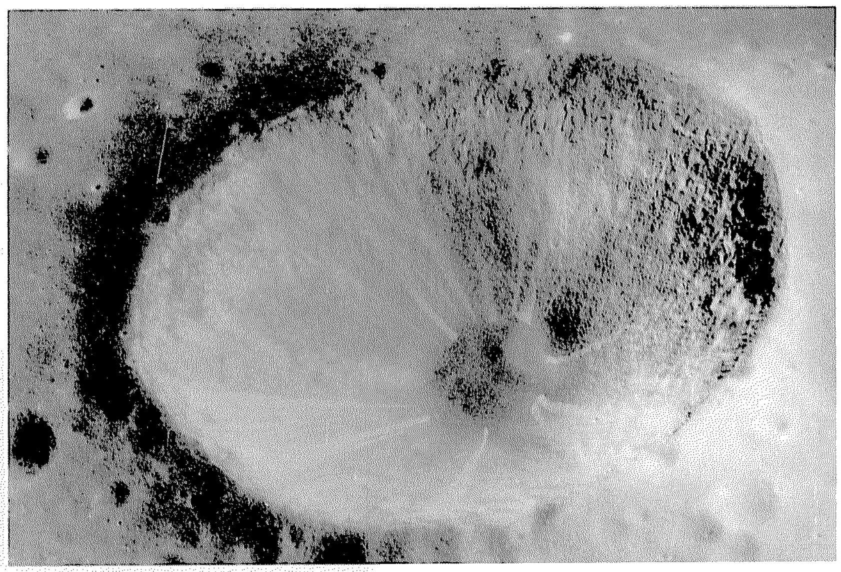

FIGURE 3.31.—Bright streaks of fresh material and darker, longer-stabilized material on wall of crater Lalande A (13 km, 6.5° S., 10° W.). Floor is composed of material already accumulated by similar downslope movement. Apollo 16 frame P–5400.

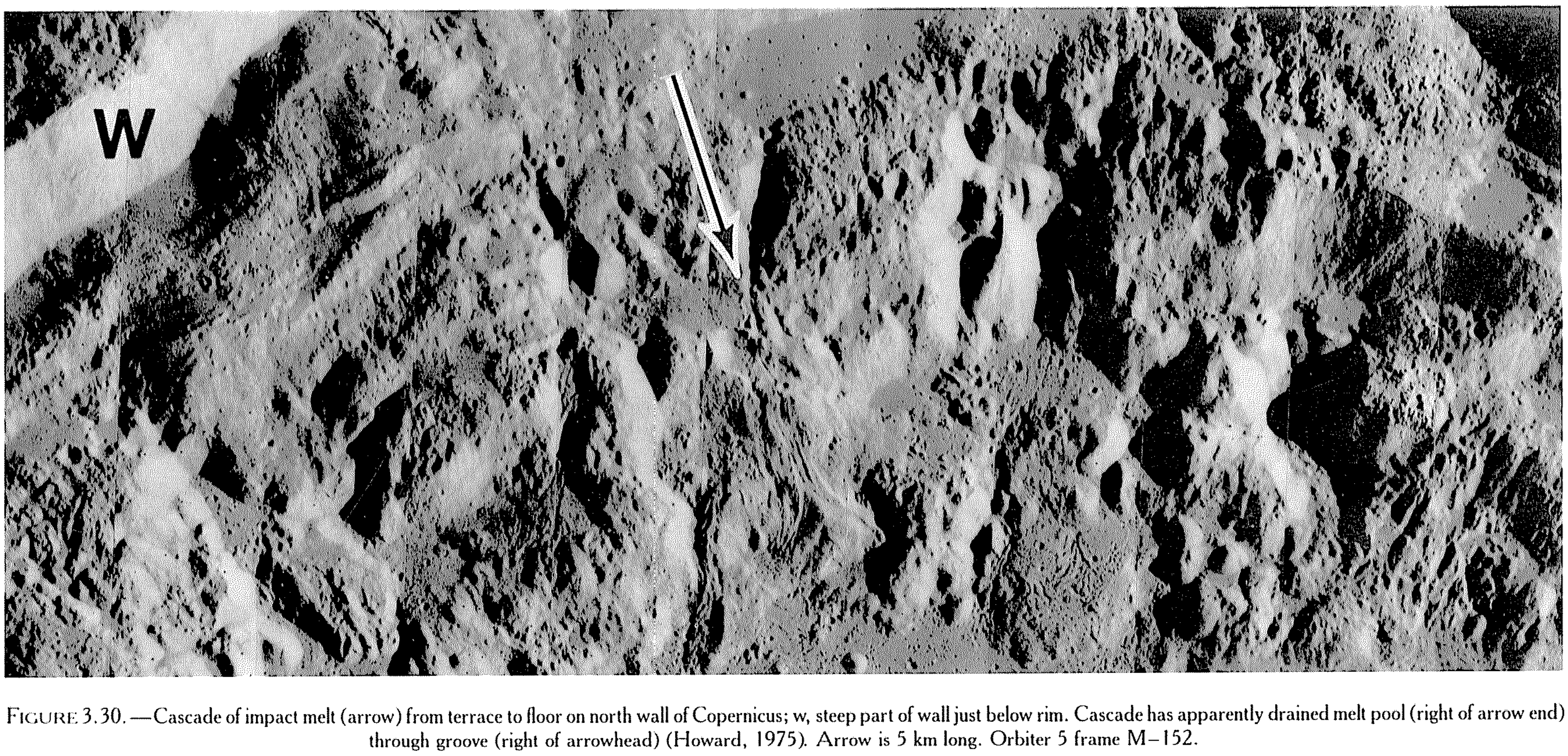

FIGURE 3.30.—Cascade of impact melt (arrow) from terrace to floor on north wall of Copernicus; w, steep part of wall just below rim. Cascade has apparently drained melt pool (right of arrow end) through groove (right of arrowhead) (Howard, 1975). Arrow is 5 km long. Orbiter 5 frame M–152.

deformation of the central part of the target. The violent and extreme uplift suggested by several lines of evidence given above seems to be supported by the observation by Murray (1980) that some peaks seem to have toppled over the crater rim (fig. 3.34). Because of the intense deformation, peaks are structurally complex. Few, if any, peaks are volcanic constructs accumulated after cessation of cratering, contrary to the interpretations presented on many geologic maps and in much other earlier lunar literature.

Floor material

Some floor materials are coeval with peak materials, some slightly younger, and some much younger. Floor materials are diverse, and photographs should be consulted during their reinterpretation. Some constitute peaklike uplifts (figs. 3.33, 3.35), which in many craters form an approximately annular pattern that foreshadows the larger rings of basins (fig. 3.2*E*; chap. 4). Separation of such lumps from central peaks may be more a matter of scale-dependent mapping convention than of genetic significance. Some hummocky floor materials bridge the gap between peak and wall, and may represent the toes of inward-displaced wall slivers or parts of the floor uplift (figs. 3.2*E*, 3.23, 3.29; Howard, 1975). Other floor materials consist of debris from the walls (figs. 3.31, 3.33).

Impact melt, formerly believed to be volcanic, partly covers many crater floors. Fissured floor materials that appeared on Lunar Orbiter 5 photographs of such young craters as Aristarchus, Tycho, and Copernicus (figs. 3.2*D*, 3.35) clearly were originally molten, and in the spirit of the times, many workers once considered them to be volcanic (Offield, 1971; Strom and Fielder, 1971; Pohn, 1972; Schultz, 1976b, p. 72). Some smooth floor materials (fig. 3.32) and other plains materials (figs. 3.2*D*, 3.36) retained volcanic interpretations longer than any other geologic-map units. The smooth "ponds" are superposed on the floor, wall, and rim, and thus were mapped not as crater materials but as special postcrater units (Milton, 1968a; Wilhelms and McCauley, 1971); they were commonly ascribed to volcanic extrusions released or localized by the impact (Strom and Fielder, 1971). However, these smooth and fissured materials have been identified as impact melt by detailed observations of the freshest and best photographed craters (figs. 3.23, 3.36; Shoemaker and others, 1968; Howard, 1975; Howard and Wilshire, 1975; Hawke and Head, 1977a; Gault and Wedekind, 1978). Impact melt veneers much of the crater interior and rim, and is ponded in favorable depressions (fig. 3.36). Fissures that continue from the floor over many of the floor uplifts indicate that melt rock coats these uplifts as well (fig. 3.35; Howard and Wilshire, 1975). The fissures and many irregular pits suggest drainage of impact melt into underlying porous breccia (fig. 3.35; Howard, 1975), not volcanism (Hartmann, 1968). Some melt flows came to rest later than the peak (fig. 3.32), in confirmation of terrestrial observations indicating that peak formation is even quicker than melt solidification. The only internally generated materials associated with craters are the mare materials that flood many craters and, possibly, small amounts of other material, such as that in the floor of the endogenic crater Hyginus (Pike, 1976).

Impact-melted floor materials probably would provide a chemically representative sample of the target rocks because target materials are extensively homogenized during impact melting (Dence, 1971; Grieve and others, 1974; Grieve, 1975; Simonds and others, 1976a, b). Conversely, the material on older crater floors may be completely unrelated to the crater that contains them or to the subcrater material (Aliacensis, fig. 3.26). Even craters that lack recognized deposits of mare basalt or ejecta may be filled by debris derived from the walls or introduced gradually as fragments by random distant impacts. Such slowly accumulated floor materials may yield random samples of large parts of the lunar surface.

In summary, geologic mapping of the materials of lunar craters has proved to be generally accurate in delineating significant units and determining mutual age relations, but the interpretations of many mapped units have changed. The absolute-age differences detected among crater-material facies by stratigraphic relations have shrunk from millions of years to minutes. The materials have moved continuously closer to an almost exclusive impact interpretation and away from volcanic or hybrid interpretations, under the prodding of sample analyses and continued photogeologic, Earth-analog, and experimental studies.

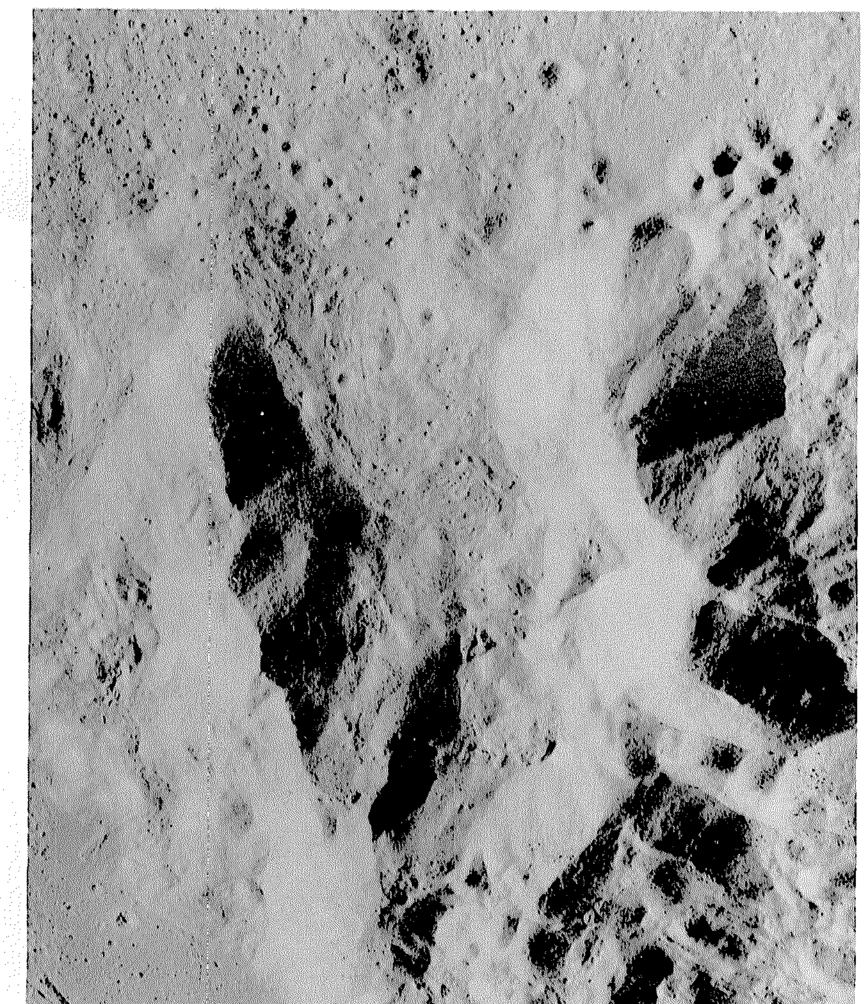

FIGURE 3.32.—Part of "lobster claw" peak of crater King (compare fig. 3.23*A*), showing superposition of impact melt in gap of peak. Apollo 16 frame P–4998.

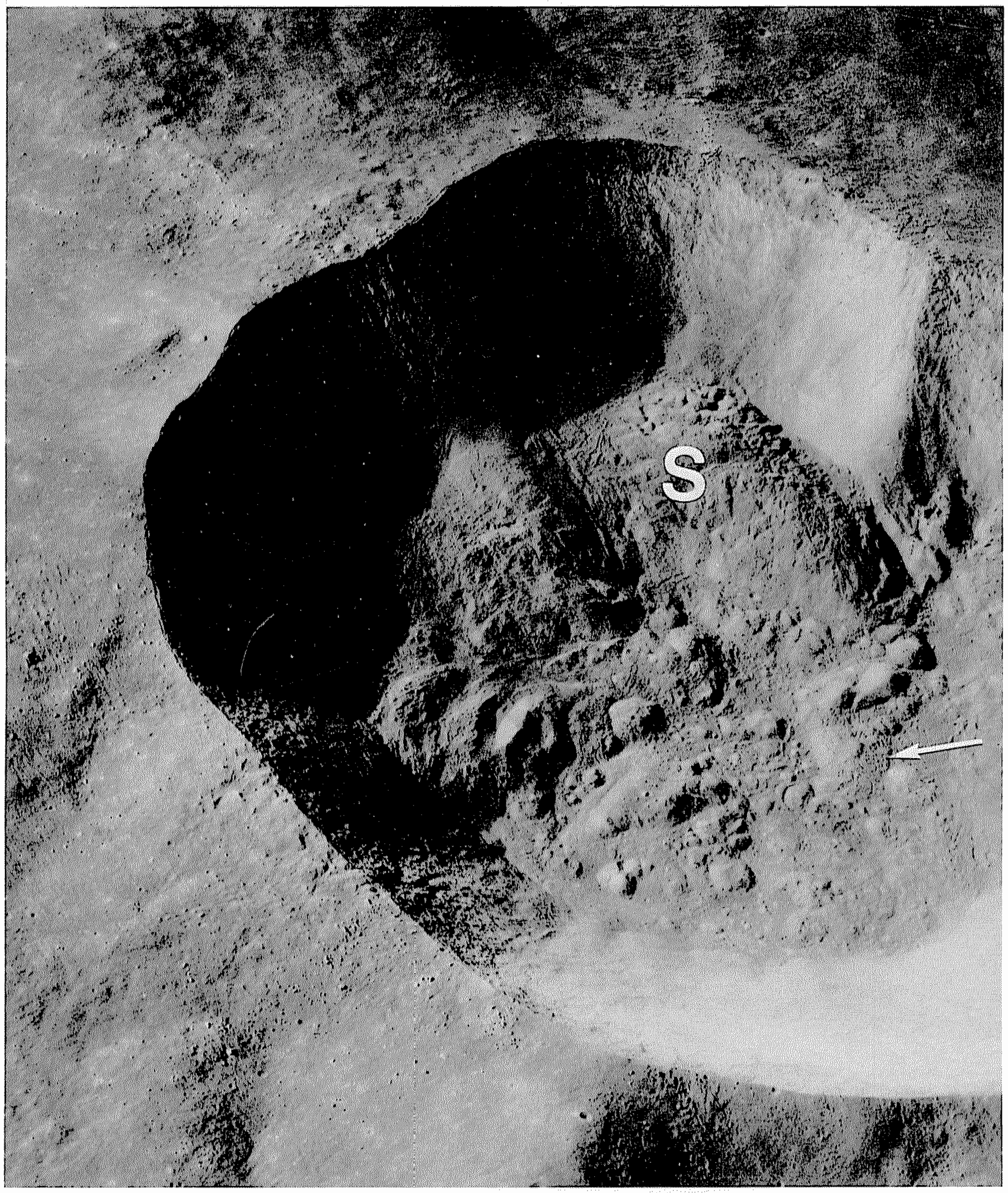

FIGURE 3.33.—Crater Proclus (28 km, 16° N., 47° E.), showing terrace-free walls, slump from upper wall (S), coarse floor mounds probably produced by floor uplift, and fissured impact melt on floor (arrow). Apollo 17 frame P–2265.

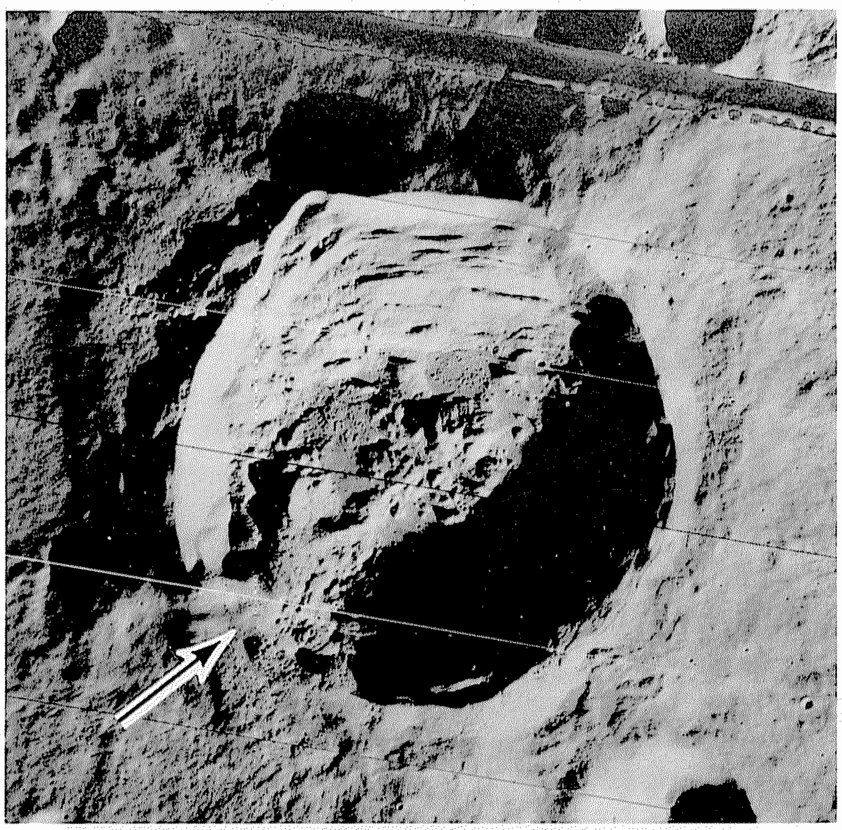

FIGURE 3.34.—Crater Anaxagoras (51 km, 73° N., 10° W.). Peak material apparently toppled over rim at arrow (Murray, 1980). Orbiter 4 frame H–128.

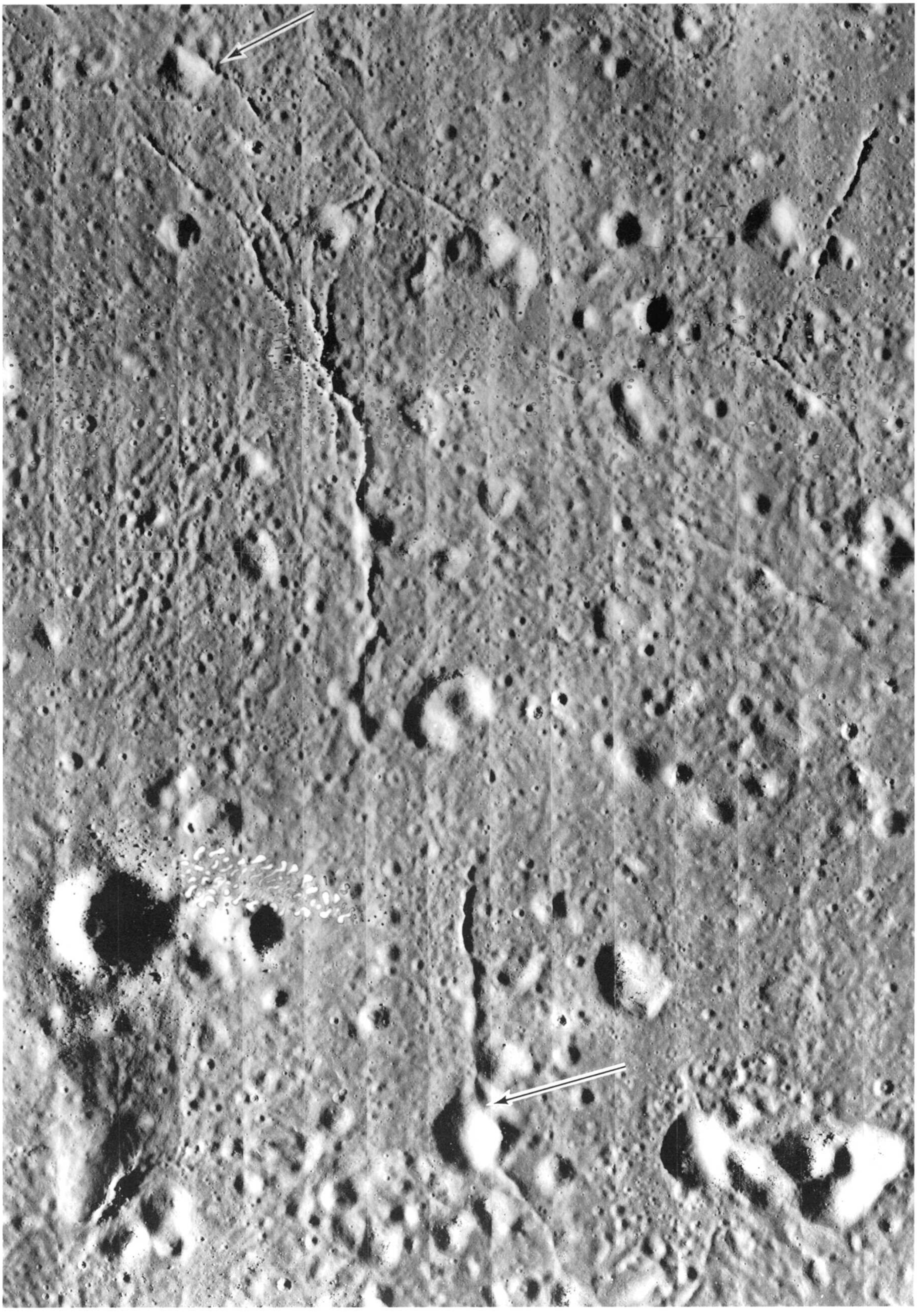

FIGURE 3.35.—Impact melt and floor mounds of Copernicus; melt is superposed on mounds at arrows. Fissures indicate shrinkage of melt and, possibly, drainage into subsurface cavities. Orbiter 5 frame H–153.

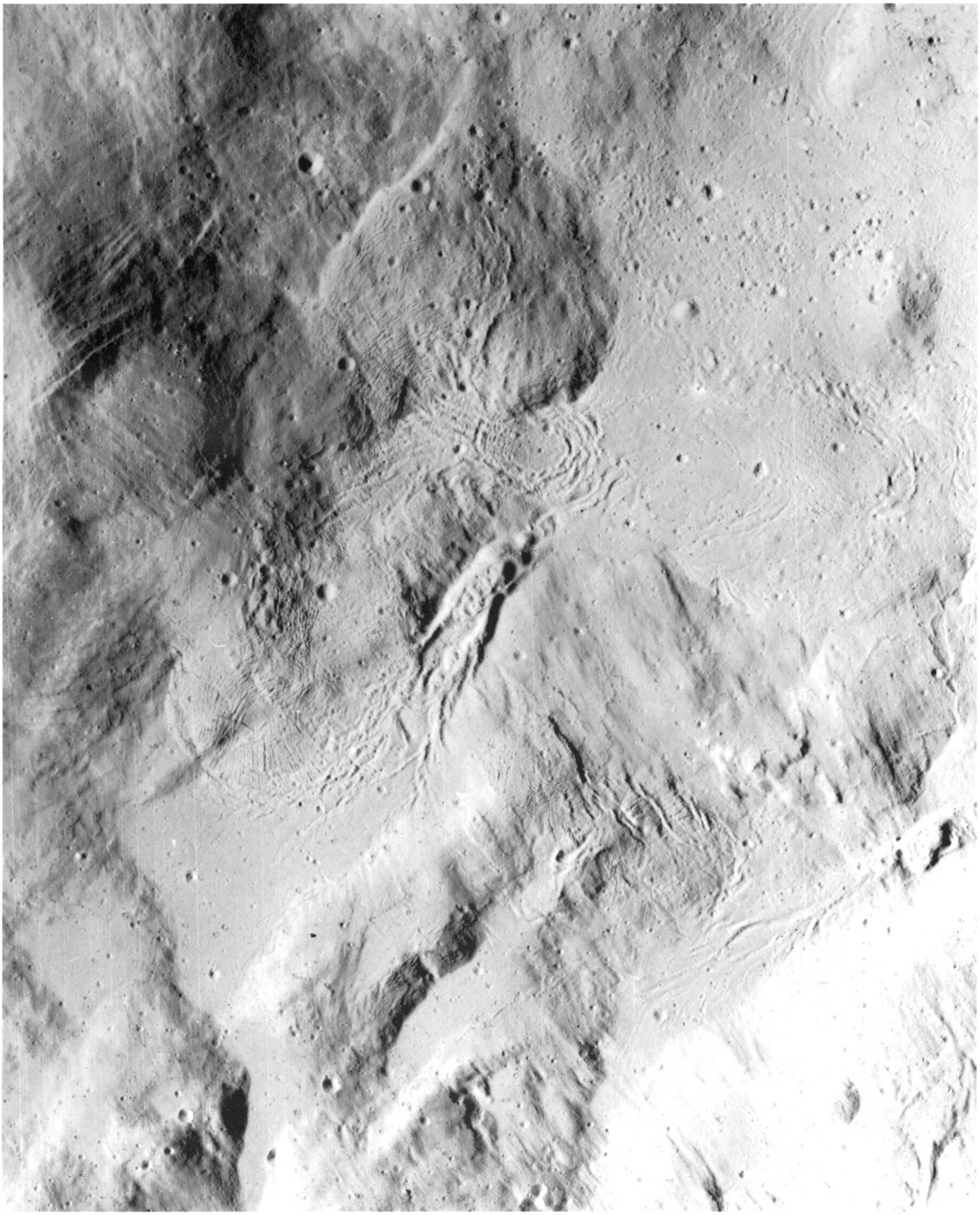

FIGURE 3.36.—Lineations and festoons indicating flow of impact melt in exterior pool of crater King (fig. 3.23*A*). Melt has flowed over rim material and collected in depressions (Howard and Wilshire, 1975). Apollo 16 frame P–5000.